Spectroscopic study of the Moses Lake dune field, WA: Determination of compositional distributions and source lithologies

Joshua L. Bandfield

Laboratory for Extraterrestrial Physics
NASA Goddard Space Flight Center

Kenneth S. Edgett

Malin Space Science Systems

Philip R. Christensen

Department of Geological Sciences
Arizona State University

Send correspondence to:

Joshua Bandfield
Code 693.0
NASA Goddard Space Flight Center
Greenbelt, MD 20771

Phone: (301) 286-3962
Fax: (301) 286-0212
e-mail: jbandfield@lepvax.gsfc.nasa.gov

Abstract

Source lithologies and transport histories of materials within the Ephrata Fan are investigated. Data were collected using a variety of remote sensing, laboratory spectroscopic, and field observations and techniques. Laboratory thermal emission spectra were collected of bedrock within the Grand Coulee, dune samples, and clast deposits. Factor analysis, target transformation, and endmember recovery techniques were applied to the set of dune samples as well as a set of grain size fractions. The dune sample spectra are composed of three components that represent basalt, granodiorite, and clay compositions. The basalt and granodiorite components are similar to spectra of clast and bedrock samples from the Grand Coulee and the Ephrata fan. The clay component is similar to weathering surfaces located within the dune field. The same components were recovered from the set of grain size fractions from a single dune sample demonstrating a relatively higher basalt concentration with grain sizes >~250μm. Thermal Infrared Multispectral Scanner (TIMS) data display significant intra-dune compositional variation and no discernable inter-dune compositional variation, indicating that the basalt and granodiorite components were likely deposited simultaneously and subsequently separated by wind based on grain size. Basalt and granodiorite bedrock units within the Channeled Scablands are source materials for the deposits within the Ephrata Fan and Moses Lake dune field. The Columbia River, located 20 km west of the dune field, is not a likely source of material.

Introduction

Martian eolian dunes and catastrophic flood deposits are considered to be useful tools from which geologic histories and martian lithologic properties may be discerned via orbital and in situ remote sensing. For example, in 1997 the Mars Pathfinder spacecraft landed on a plain covered by flood deposits from Ares and Tiu Valles with the intent to learn something about the composition of the cratered highland rock through which these valleys are cut [*Golombek et al.*, 1997, 1999]. Likewise, from orbit, sand dunes offer relatively dust-free surfaces composed of grains typically 100-500 μm in size [*Edgett and Christensen*, 1991] that can be observed via multispectral infrared instruments to determine mineral or lithologic composition [e.g., *Blount et al.* 1990; *Ramsey et al.* 1999; *Edgett* 1994a]. Indications from the Thermal Emission Spectrometer (TES) aboard Mars Global Surveyor (MGS), for example, suggest that dunes in the martian north polar region have a composition that is more silicic than those in the southern highlands---those in the north can be considered as andesitic, while those in the south can be classified as basaltic [*Bandfield et al.*, 2000a; *Christensen et al.*, 2000a,b].

The MGS TES has been in orbit around Mars since September 1997 and is expected to continue to collect high spectral resolution observations in the 200-1650 cm^{-1} (6 to 50 μm) range through at least April 2002. A second orbiter, 2001 Mars Odyssey, carrying the 9-channel Thermal Emission Spectral Imager (THEMIS) finished aerobraking at Mars in January 2002. In 2003, the Mars Exploration Rovers (MER) will be sent toward Mars, each carrying a mini-TES to obtain spectra of rocks and regolith from a vantage point near the surface. With these thermal infrared experiments in mind,

particularly the MGS TES and Odyssey THEMIS, a terrestrial eolian dune field was sought in 1990 as a potential test-bed for validating algorithms and approaches to analysis of thermal infrared spectra from Mars.

Prior to the MGS mission, all ground-based and orbiter based evidence suggested that martian dunes would be mafic rather sialic like their quartz-rich counterparts on Earth [see discussion in *Edgett and Lancaster*, 1993]. The largest known basaltic dune field on Earth is located in the Moses Lake, Washington, area in western North America. Petrographic analysis by *Petrone* [1970] suggested that the dune sand at Moses Lake is a mixture composed mainly of basalt lithic fragments and quartz grains. These two very different materials were considered to form a simple two-component mixture that could be used to begin to test some of the spectral analysis techniques that were being developed during the 1990s for application to Mars thermal infrared data.

This paper is an initial analysis of Moses Lake dune sand in the context of using thermal infrared spectra and remote sensing observations. These data are applied to the testing of a specific, focused hypothesis. In his thesis, *Petrone* [1970] concluded that there are two sources for the sand comprising the Moses Lake dunes: 1) in-situ reworking and subsequent downwind transport of basaltic sand originally deposited by the catastropic Spokane or Scabland floods, and 2) windblown transport to the basaltic dune field of ~95% quartz sand from the Columbia River bed located in a gorge roughly 20 km from the nearest present-day dune field. This study tests Petrone's conclusion regarding a Columbia River source, and finds 1) that the windblown sands in the adjacent Columbia River gorge are not as quartz-rich as Petrone had concluded, and 2) that the types and

abundances of materials comprising the Moses Lake Dunes are more consistent with an origin entirely by eolian reworking of Scabland flood sediment transported and in large part derived from within the Grand Coulee channel located approximately 30 km north of the dune field.

Ramsey et al. [1999] has shown the ability of thermal infrared remote sensing data to greatly facilitate the determination of spatial distributions and sources of mineralogical eolian units. Previous work is expanded upon here by demonstrating the ability to interpret a more complex spatial distribution of mineralogical composition that does not demonstrate a clear geographical relation to any source. In addition, the spectral signature of mineralogical units that are independently variable, but are mixed at the scale of the spectral measurement, may be isolated without physically separating the sample. This ability to isolate compositional units is important with remotely sensed data where spatial sampling is on the order of meters to kilometers, as well as laboratory data where separation of mineralogical units may be inaccurate as well as tedious and time-consuming as in the case of a mixed sand.

The combination of in-situ field observations, remote sensing data, and laboratory measurements are complimentary methods that allow for a much clearer interpretation of a scientific problem than any of these methods would individually. The TIMS data used in this study is excellent for distinguishing compositional units and providing their spatial distribution over large areas that might not be easily sampled or accessed [*Kahle*, 1987; *Gillespie*, 1992; *Weitz* and *Farr*, 1992; *Hook* et al, 1994; *Crowley* and *Hook*, 1996; *Ramsey et al.*, 1999; *Ramsey* and *Fink*, 1999]. In-situ field observations provide textural

and relational observations in addition to adding confidence to both remote sensing and laboratory data interpretations. The laboratory measurements provide quantitative compositional information that cannot be achieved through either visual analysis or the limited spatial and spectral resolution of the remote sensing datasets.

Geologic and Temporal Setting

The Moses Lake dune field is located in the southern Quincy Basin of central Washington state, largely south and west of Moses Lake, north of the Frenchmen Hills, and south of U.S. Interstate Highway 90 (Figure 1). The Quincy Basin is a structurally-controlled depression formed within the Tertiary Yakima Basalt Subgroup of the Columbia River Basalt Group. Much of the basaltic dune sand is considered to have been reworked from sediment deposited in the Quincy Basin during one or more of the multiple Lake Missoula or Channeled Scabland flood events that swept across eastern Washington and the underlying Columbia Basalts between 17,000 and 12,000 years ago [*Bretz et al.*, 1956, *Nummedal*, 1978]. These multiple flood events, caused by the catastrophic breaching of an ice dam at Lake Missoula, created a landscape that is known today as the Channeled Scabland, the biggest channel of which is the Grand Coulee that runs several hundred kilometers from northeastern Washington to the Ephrata Fan in northern Quincy Basin. *Bretz* [1969] proposed that there were at least eight separate flood events, others have suggested that there were as many as 40 to 100 events [see *Baker and Bunker*, 1985; *Waitt et al.*, 1994]. The dunes (Figure 2) are located at the distal end of the Ephrata Fan, a broad expanse of boulders, cobbles, and gravel deposited by

one or more of the Missoula Floods [*Bretz et al.*, 1956; *Rice and Edgett*, 1997]. The Ephrata Fan begins just south of Soap Lake at the southern end of the Grand Coulee (Figure 1). Water from the Scabland floods poured through a narrow constriction point and then expanded out into the Quincy Basin, forming the fan-shaped deposit. Boulders up to 18 m in size are found near and just south of this constriction point [*Bretz et al.*, 1956; *Edgett et al.*, 1995a, pp. 46-48], but the deposit fines southward into gravels, and, at Moses Lake, sand. The clasts that make up the Ephrata Fan, at least at the surface, are dominated by basalt lithics with lesser amounts of granodiorite [*Gulick*, 1990; *Rice and Edgett*, 1995], both of which outcrop within the Grand Coulee (the granodiorite lies beneath the basalts). Several images of the coulee, clasts, and dunes are shown in Figure 3.

The climate in the Quincy Basin area has been arid and semi-arid since the Missoula floods, as documented in two studies of the post-Missoula dune field 40 km south of the Moses Lake dunes on the Hanford Nuclear Reservation [*Smith*, 1992; *Stetler*, 1993]. Late Pleistocene and Holocene winds have driven the Moses Lake sands east-northeastward. Today, much of the Moses Lake dune field occurs stratigraphically above the gravels and cobbles of the central and eastern portions of the distal Ephrata Fan, which in turn lies above a scabland of eroded Wanapum Basalt units [*Grolier and Bingham*, 1971; *Gulick*, 1990]. The eastward advance of the dunes eventually dammed a portion of Rocky Ford Creek to create Moses Lake.

The dunes from a distance on a sunny day appear to be brown to blue-black in color; hand samples are nearly black with minor amounts of lighter-toned or white grains.

Petrone [1970] found the sands to generally consist of more than 55% basalt lithic fragments; lighter-toned grains comprising most of the remaining bulk were interpreted as quartz on the basis of binocular microscope analysis. Other lithic fragments cover a range of compositions including small pieces of schists transported first by glaciers then by Missoula Floods from somewhere on the Canadian Shield. The Moses Lake dune field might be the largest basaltic eolian sand accumulation on Earth [*Edgett and Lancaster,* 1993].

Using the terminology of *McKee* [1979], the dunes include parabolic and crescentic forms which are active today. The dunes' rate of advance is thought to have been significantly slowed during the past century---on the basis of eyewitness anecdotes, multi-year aerial photograph analysis, and dune positions in 1992 relative to Mount St. Helens tephra deposits from 1980 on interdune surfaces [*Petrone,* 1970; *Edgett*, 1994b].

With the Columbia Basin Project, the Moses Lake dune field became subject to a rising water table [*Walters and Grolier,* 1960, p. 16] and creation of wetlands on May 29, 1952, when the first irrigation water from the Grand Coulee arrived in the dry ditches near Moses Lake [*Holbrook,* 1956, p. 318]. The O'Sullivan Dam was emplaced in 1952, forming a catchment for irrigation runoff that flooded a large fraction of the dune field and created the Potholes Reservoir. Dunes west of the reservoir became much more wet and vegetated, although some fraction of each of the larger dunes remained subject to further downwind movement. Dunes east of the reservoir remained largely unvegetated because of their higher elevation above the water table, but the supply of sand from the west was diminished and local farmers attempted to stabilize the dune field with bales of

hay and planted grasses [*Petrone*, 1970]. Dune activity was further affected by the May 18, 1980, explosive eruption of Mount St. Helens. The region including the Moses Lake dune field received some of the thickest (2-3 cm) deposits of silt- and clay-sized tephra [*Sarna-Wojcicki* et al., 1981]. While most dunes eventually lost their covering of tephra, some smaller dunes and dune ridges have remained covered and developed a crusted surface that persisted well into the 1990's [*Edgett*, 1994b]. Larger dunes continued to advance at an estimated ~3 m/year based upon field observations in 1992 and 1998 based on measurements of dune slip faces relative to a 6-cm-thick layer of 1980 tephra preserved and visible within the location of the 1980 slip face [*Edgett*, 1994b].

Dune activity at Moses Lake was further affected in the 1980's and 1990's by additional changes in land use. Most of the dune field south and west of Moses Lake and the Potholes Reservoir is now a wetland and wildlife preserve. The dunes occurring east of the Potholes Reservoir have been subject to other, human-induced effects that generally stabilized or destroyed the dunes. However, a small portion of the dune field between northeastern Potholes Reservoir and southern Moses Lake is reserved for recreational vehicle traffic. This area remains the most geologically active portion of the dune field because the vehicles prevent vegetation from growing.

Approach

Several datasets and analysis techniques were used to both gain an understanding of the processes in effect in the Ephrata fan and evaluate the effectiveness of the techniques themselves. Remote sensing data collected includes simultaneously collected airphotos and TIMS imaging data that cover much of the dune field and extend to the Columbia

River to the west. A hardcopy Landsat scene of the entire Ephrata fan area was also acquired. Samples of dune sand, clast deposits, and bedrock were also collected as well as field observations. Thermal emission spectra of the collected samples were obtained in the laboratory.

A variety of techniques were used to evaluate the datasets. Observations were made in the field, of hand samples, and airphotos to provide a visual inspection of the area and a qualitative determination of composition and texture of samples. The TIMS data were processed using a standard decorrelation stretch in order to visually enhance surface compositional variations [Gillespie *et al.*, 1986]. The laboratory spectra were evaluated using qualitative comparisons, factor analysis and endmember recovery [*Bandfield et al.*, 2000b], and deconvolution techniques [*Ramsey and Christensen*, 1998; *Ramsey et al.*, 1999].

TIMS data were acquired on July 13, 1992 (site 9224, lines 1-4) at ~4m/pixel resolution of the entire dune field. Because no atmospheric information was obtained simultaneously with the TIMS data, a standard mid-latitude summer atmospheric model was used with MODTRAN [*Berke et al.*, 1989] to provide an atmospheric correction. A decorrelation stretch image using TIMS bands 5, 3, and 1 projected as red, green, and blue respectively was produced similar to that of *Ramsey et al.* [1999]. A subset of the image that contained only the dune field was used to provide the rotation and stretch for the entire dataset. This was done in order to maximize the contrast within the dune field rather than the farmland, volcanic ash, and water that form the majority of the TIMS dataset but are not the focus of this study.

Initial field reconnaissance and sample collection was conducted by K.S.E. from September 30 through October 6, 1990. This was followed by a more extensive field sampling by K.S.E. August 19-27, 1992. The 1992 goal was to sample a large number of dunes over the entire dune field. Samples from 14 different dunes were collected in 1990, and 50 individual dunes were sampled in 1992.

Samples were taken by scraping grains from the upper 2-5 mm of the surface over an area approximately 0.5 by 0.5 m and placing them in sealed, airtight plastic bags for transport back to the laboratory. For uniformity, samples from the crest of each dune sampled were collected in this manner. For several dunes, additional samples were collected at various places on the stoss and slip face slopes (again, upper 2-5 mm over 0.5 m area).

A second set of field observations and samples were acquired by J.L.B. during April of 1998. The focus of this second sample collection was of larger clast size samples in the Ephrata fan, bedrock samples from the Grand Coulee, and dune samples from the Columbia River. Each of these areas was investigated as possible sources of the dune material and samples were taken for laboratory spectral acquisition. Dune samples were collected from the top 5 mm of the surface and rock samples were broken in order to retrieve both a fresh and weathered surface on each sample.

Laboratory spectra were acquired and calibrated using the method 1 of *Christensen and Harrison* [1993] as modified by *Ruff et al.* [1997] using a Mattson Cygnus spectrometer equipped with a KBr beamsplitter and a DTGS detector. Spectra were obtained between 2000-400 cm^{-1} (5-25 μm) at a sampling interval of 2 cm^{-1}. Dune

samples were poured into a ~3 cm diameter and 0.5 cm deep copper cup which was actively heated to a temperature of 80 C during spectral acquisition. Hand samples were heated to 80 C and are not actively heated during spectral acquisition. 180 scans were acquired of each sample over a ~5 minute period and averaged to improve the signal to noise ratio. *Ruff et al.* [1997] extensively analyzed possible sources of error in this technique and determined a precision of better than 1% emissivity and accuracy of better than 2% absolute emissivity.

Because the hand samples were constantly cooling during spectral acquisition there was some concern of possible effects introduced in the spectra due to the anisothermality. To verify that this was not a significant effect introduced in the spectra, three spectra were acquired using only 60 scans each over a ~5 minute period. These spectra were averaged before calibration to simulate the standard 180 scan spectral acquisition procedure as well as individually calibrated in order to significantly reduce the amount of temperature change during spectral acquisition. The result verified that the sample temperature change during acquisition of the spectra does not have a significant effect on the calibrated spectra.

Spectra of samples taken from the top 2-5 mm of the crest of 39 dunes covering the extent of the dune field as well as a set of 6 grain size fractions were run separately through a spectral factor analysis and endmember recovery technique described by *Bandfield et al.* [2000b] and summarized below. This is a combination technique that uses factor analysis (R-mode, mean removed) and target transformation as adapted from *Malinowski* [1991] used as a spectral endmember recovery technique that allows for

isolation of spectral endmembers from a set of mixed data [*Bandfield et al.*, 2000b]. Factor analysis provides an indication of the complexity of the dataset, including the number of independent endmember components within a dataset. The endmember recovery technique provides the ability to recover the spectral shape of endmembers from a set of mixed spectra even if the exact endmember is not present in a set of reference spectra.

Factor analysis derives the eigenvalues and eigenvectors from the set of mixed spectra to determine the number of components that influence the system. The eigenvalues that correspond to each of the derived eigenvectors describe the amount of variance contributed to the system along the axis parallel to the eigenvector. The value of this analysis is the reduction of multi-dimensional data into just a few dimensions. For example, if there are only three components varying within a system, the system can be reconstructed within the limits of the noise present with linear combinations of the first three eigenvectors.

The maximum dimensionality that can be spanned by the spectra is the number of spectral endmembers. Because the number of spectral bands in the laboratory data (usually >100's) greatly exceeds the number of significant endmember components (typically less than 5), the spectra will lie in a space contained within the higher dimensionality of the dataset with a number of dimensions equal to the number of endmembers. As the derived eigenvalues and eigenvectors account for any variation as efficiently as possible, the first **n** eigenvectors, where **n** is the number of spectral endmembers present, will span this space that is also spanned by the data [*Malinowski*,

1991]. This indicates that all the data and the spectral endmembers may be reconstructed by linear combinations of these first eigenvectors.

Target transformation is a test for the fit of a possible spectral endmember to the set of mixed spectra. If the possible endmember, called the trial spectrum, is a spectral endmember, then the trial spectrum is contained within the space spanned by the significant eigenvectors. As a result, the trial spectrum may be reconstructed as a linear combination of the significant eigenvectors. To determine whether or not a trial spectrum is contained within the eigenvector space, a combination of eigenvectors are fit to the test spectrum in a least squares manner and the test and eigenvector combination, called the best-fit spectrum, are compared to determine their similarity. The target transformation is performed on each trial spectrum separately, which allows the determination of individual endmembers independent of the determination of others [*Malinowski*, 1991; *Bandfield et al.*, 2000b].

Inspection of the best-fit spectra from the target transformation for numerous test cases show that even for many failed transformations, where the best-fit and trial spectra are not similar, the best-fit spectrum is an accurate spectral endmember [*Bandfield et al.*, 2000b]. For successful target transformation trials, the best-fit spectrum is a refined and more accurate endmember than the trial spectrum. The endmember recovery technique takes advantage of this property in the analysis of a dataset by allowing for the recovery, in addition to confirmation, of the set of true spectral endmembers for the system from a group of best-fit spectra that result from the target transformation. There is no automatic system for this selection and both human experience and bias are introduced with the

selection of these endmembers. However, as discussed below, the validity of this selection may be checked. These recovered endmembers may be analyzed further for their properties and mineralogical compositions.

Obtaining a spectral endmember using a trial spectrum that is not necessarily similar to the best-fit spectrum is demonstrated in *Bandfield et al.* [2000b]. Because the target transformation is simply fitting the trial spectrum with a linear combination of eigenvectors in a least squares manner, there is no uniqueness of one combination over another. Spectral shapes of substances are broadly similar to each other, however, and the trial spectra produce realistic spectral shapes from the eigenvectors even if the specific spectral endmember is not present in the set of trial spectra. Because endmembers show a greater spectral contrast than mixtures (i.e. features are more pronounced), the target transformation method is practical for obtaining the endmembers present in a system. The target transformation matches as well as possible the relatively high spectral contrast present in the trial spectrum by fitting a combination of the eigenvectors to the trial. As a result, best-fit spectra are often spectral endmembers. Spectral endmembers are generally recovered with trial spectra that contain absorptions near the same wavelengths as the spectral endmembers, but these absorptions are not necessarily the same shape.

The ability to obtain endmembers through the best-fit spectra does necessitate the use of a spectral library, but endmembers present in the library need only be broadly similar in band position and shape to those in the data. Small variations in features are recovered in the best-fit spectra. If the spectral endmember is not present in the trial set, it may be

recovered in the best-fit spectrum of a trial spectrum that is only approximately similar in shape to the endmember [*Bandfield et al.*, 2000b].

It has been shown that the thermal infrared spectrum of a mixed surface may be closely modeled using a linear combination of the endmember spectra weighted by the aerial concentration of each endmember [*Adams et al.*, 1984; *Thomson* and *Salisbury*, 1993; *Ramsey* and *Christensen*, 1998; *Ramsey et al.*, 1999]. The deconvolution provides a linear least squares fit of the measured spectra using combinations of the recovered endmember spectra and the weightings represent the component abundances [*Ramsey* and *Christensen*, 1998]. It also provides an independent check on the validity of the selected spectral endmembers. If the selected endmembers are correct, then the component sums will be unity, RMS error between the measured and modeled spectra will be approximately equal to the RMS noise level of the spectra, and the component percentages will be between 0 and 100%. An additional check on the validity of the spectral endmembers is to verify their linear independence. This check is done by confirming that no selected endmember can be modeled as a linear combination of the other endmembers selected.

The recovered endmembers from the dune sample sets were compared to spectra of samples taken from larger clasts, bedrock, and dunes near the Columbia River to determine their mineralogical similarity. The TIMS data and in-situ observations were used to identify possible sources and spatial distributions of these materials.

Results

Introduction

The focus of the analysis is on the components, composition, and spatial distribution of the bedrock, clasts, and sand in order to determine the sources and distributions of the materials deposited on the Ephrata fan. The results will be separated into observations and spectral characteristics of the bedrock units and large clasts followed by a spectral analysis of the dune samples. The spatial distribution of the source materials for the dunes is shown using the processed TIMS image in addition to analysis of the spatial distribution of spectral characteristics of the dune samples using the laboratory spectra.

Bedrock lithology

Bedrock units are visible towards the north and northeast in the walls of large channels cut by the floods. The largest of these channels, the Grand Coulee, was inspected and sampled for possible source materials that are distributed throughout the Ephrata Fan. The mouth of the channel lies ~30 km north of the dune field. The walls of the channel consist of massive to vesicular basaltic layers from lava flows. These walls consist of the Wanapum and Grande Ronde units of the Columbia River Basalt Group that is regionally widespread and is the only compositional bedrock unit visible in the area within ~60 km north (upstream) of the channel opening [*Stoffel et al.*, 1991].

Farther up the channel, the bedrock type transitions from basalt to an underlying granodiorite unit. The mineralogy of the granodiorite unit is dominated by a predominance of biotite, quartz, and plagioclase that has a ‘salt and pepper’ texture and appearance. Other textures and compositions within the granodiorite unit are present as

well including a gneissic texture that concentrates the biotite in bands and local areas with a much increased potassium feldspar content with crystals of up to ~3 cm in diameter. No other bedrock types are present within the Grand Coulee to the Coulee Dam, ~75 km north of the channel mouth, with the exception of minor outcrops of Oligocene metasediments ~100 km up the channel [*Stoffel et al.*, 1991].

Large clasts

Several sites within the Ephrata Fan between the mouth of the Grand Coulee and the dune field were inspected and sampled to obtain the distribution and composition of the larger clasts (pebble to boulder sized) interpreted to be deposited by the floods. These observations found only granodiorite and basalt clasts to be present. The clasts are similar in appearance and composition to the two major bedrock units present within the Grand Coulee. Most clasts are well rounded and weathered. These weathering surfaces give the granodiorite clasts a dark color comparable to the basalt clasts.

The size distributions of the two clast types are noticeably different. Basaltic clasts are common in a size range between several centimeters to several meters in diameter and were seen up to ~10 m in diameter. The granodioritic clasts are commonly ~1 to several meters in diameter, though several smaller clasts were found. Visual estimates at the sites examined place the concentration of granodioritic clasts >1 m in diameter at ~25% and the percentage <1 m in diameter at <1%. Basaltic clast size generally decreases with distance from the channel mouth, though there are localized concentrations due to the formation of bars by the floods. However, no large concentration of granodioritic clasts

<1 m in diameter was found. The reason for the differences in clast size distributions between the basalt and granodiorite compositions is unclear.

Spectral Characteristics of Clasts and Bedrock

The spectral characteristics of the fresh surfaces of both the granodiorite and basalt compare well with samples of similar mineralogy analyzed by *Feely* and *Christensen* [1999] (Figure 4). The granodiorite samples show the characteristic silicate absorptions dominated by quartz at short wavelengths between 1000-1200 cm^{-1} as well as several narrow absorptions at >550cm^{-1}. The basaltic samples have the typical relatively featureless bowl shaped absorption between 800-1100 cm^{-1} as well as 500cm^{-1}. Both of these compositions are identifiable by their spectra and are consistent with the visual analysis.

Weathering products and coatings are present on many of the rock samples. These are most prevalent on the clast samples that have been resting in soils that may retain moisture much longer than bedrock outcrops. In some cases, these weathered or coated surfaces may completely obscure the spectral signature of the rock (Figure 5). The spectral signature of these surfaces have a narrow absorption between 1000-1100 cm^{-1} characteristic of clay minerals such as iron smectite or montmorillonite [*Christensen et al.* 2000c].

Columbia river sands

An additional possible source material to consider for the Moses Lake dune field is sand from the Columbia River. There are several small dune fields immediately east of the Columbia River that appear to be migrating east towards the Moses Lake dune field.

These dune fields are not extensive and are separated from the Moses Lake dune field by 20 km. Spectra of the beach and dune sand as well as larger clast samples are similar to those of the fresh surfaces of granodioritic clasts and bedrock indicating similar compositions (Figure 6). There does not appear to be a large basaltic component to the sand based on both visual and spectral analysis. As granodiorite contains only ~35-50% quartz, this result is not consistent with the ~98% quartz content as determined by *Petrone* [1970] through visual analysis of Columbia River sand.

Dunes

Factor analysis was performed on the 39 spectra of dune crest samples (Figure 7) to determine how many independent spectral components are present. Because of the lack of features at short wavelengths and the increased noise level at longer wavelengths, only the 1400-450 cm^{-1} portion of the spectrum was used for the analysis. The first eigenvector (eigenvectors are shown in Figure 8) shows significant spectral-like features and the first eigenvalue indicates a significant amount of variance indicating that there are 2 (The mean, which was removed prior to the analysis, represents a component in addition to any significant eigenvectors and eigenvalues.) major components in the system.

There is also some spectral information likely due to mineralogy contained in the next 3 eigenvectors. This spectral information is minor and consistently in the same ~1000-1100 cm^{-1} region or coincident with the first eigenvector. Since the same general spectral information is repeated in the three eigenvectors, they cannot be used to describe more than one spectral component. While major components that have a large influence upon

the spectra are easily separated from the minor systematic noise components introduced into the system, such as noise in the instrument response function used for calibration, minor components are not so cleanly separated [*Bandfield et al.*, 2000b]. As a result, the results of the factor analysis are interpreted to indicate that there are two major spectral components as well as a third minor mineralogical component. Additional minor components are present, but these components represent systematic spectral point to spectral point noiselike components and do not represent realistic compositional components. This minor component may represent a composition present in small concentrations (<~20%) or a spectral component that does not have a large spectral contrast from other endmembers present in the system.

The spectral endmembers were recovered using 173 pure mineral spectra from the Arizona State University mineral library [*Christensen et al.*, 2000c] as the set of trial spectra and the significant eigenvectors that contain spectral information were fit to these spectra in a least squares manner. In addition, this trial set was augmented by a suite of rock spectra collected by *Feely and Christensen* [1999] and various rock and mineral spectra collected in the laboratory. This was done to provide as wide a variety of trial shapes as possible in order to increase the chances of endmember recovery if the exact endmember is not present in any of the trial spectra.

The endmember recovery technique was applied using the first 7 eigenvectors and the mean from the set of mixed spectra. Small overestimations of the number of components for the target transformation and endmember recovery does not have a detrimental effect on the results and ensures that all spectral information is included in the system. The

dimensionality of the dataset is still greatly reduced from ~800 (the number of spectral bands used in the analysis) to 8 and eigenvectors that contain only noise will not be preferentially used by the algorithm because combinations of small numbers of eigenvectors that contain only random noise can not adequately reproduce spectral features. The opposite is the case if the true number of spectral components is underestimated. If the system is underestimated by even one component, it may be impossible to accurately recover any spectral endmembers. As discussed above, the minor spectral information contained within eigenvectors 2-4 is true spectral information that is contained within the dataset and will be used by the algorithm to recover the spectral endmembers.

Selection of the spectral endmembers from the set of best-fit shapes was done manually. The several hundred best-fit eigenvector combinations returned from the algorithm fell into three basic categories (Figure 9): 1) unrealistic spectral shapes such as those with emissivities >1; 2) spectral mixtures that could be modeled as a mixture of positive concentrations of the spectral endmembers; 3) spectral endmembers. In this manner, three possible spectral endmember shapes were selected (Figure 10).

To obtain endmember abundances in the samples and verify that the correct endmember set was selected, the recovered endmembers were used to deconvolve the original dune crest spectra used for the analysis. A summary of this analysis is provided in Table 1. Linear combinations can reconstruct each sample spectrum extremely closely with an average RMS error between the real and modeled spectrum of 0.0018 and a maximum of 0.0027 in emissivity. All derived endmember concentrations are between 0

and 100% and the average concentration sum is 100.08%. In addition none of the three selected spectral endmembers could be modeled as a combination of the other two. These results place a high confidence in the accuracy of the recovered spectral endmembers.

Two of the recovered spectral endmembers from the dune sand sample spectra are very similar in nature to the spectra of the basaltic and granodioritic clast and bedrock samples. The spectra of the fresh surfaces of the granodiorite clasts and bedrock match well with one of the recovered endmembers, indicating that a component of sand with a granodioritic composition is independently variable (Figure 11a). The other recovered spectral endmember also matches well with the spectra of fresh surfaces of the basalt clasts and bedrock (Figure 11b). The concentrations of the granodioritic endmember vary from 15 to 38% while the range of basaltic composition concentrations varies from 53 to 76%.

The third component contains more noise than the other two and is indicative of a minor component as are the component concentrations which are <19%. This third spectral endmember is very comparable in shape to clay minerals and is similar to the spectrum of a coating on the buried surface of a basaltic clast located within the dune field (Figure 11c). Whether this spectral endmember represents a weathering product that forms on the surface of the sand particles or is present as separate particles is unclear from this analysis.

One of the dune crest samples was divided into 6 grain size fractions between 90 and 710 μm which accounted for ~99% by weight of the sample. The spectra of these size

fractions were run through the same analysis as the set of 39 dune crest spectra. Factor analysis indicates that there are 3 components as with the previous analysis. Three endmembers were recovered which are nearly identical with the previous analysis as well.

The 3 recovered spectral endmembers were used to deconvolve the original grain size spectra. Linear combinations of the three spectral endmembers can model the original spectra with low RMS errors, component concentration percentages between 0 and 100% and component concentration sums very nearly equal to 100% (Table 2).

A systematic trend is present in the deconvolution results of the grain size suite spectra as shown in Table 2. There is a clear compositional transition at grain sizes of ~250μm. The larger grain sizes (250-710 μm) contain ~28% aerial fraction granodiorite and ~62% basalt whereas the smaller grain size fractions (<250μm) contain ~38% granodiorite and ~53% basalt. The clay spectral endmember is present at concentrations of ~10% in all samples and no significant trends could be established relative to grain size.

Distributions

The derived component concentrations for each of the 39 dune crest samples were mapped to try to obtain a rough sense of compositional trends. While there appears to be substantial variation in the component concentrations, the spatial distribution of these percentages displayed no obvious regional trend. Attempts failed to locate a larger concentration of the granodiorite endmember towards the west where a possible source of granodioritic sand from the banks of the Columbia River is located. The dune migration

is towards the northeast, roughly orthogonal to the Columbia River. To test the possibility of a granodioritic source from the Columbia River, the component concentrations can be plotted as a function of distance from the river (Figure 12). There is no strong compositional trend among any of the dune components, though granodiorite concentrations do decrease slightly with increasing distance. This is opposite of what would be expected if the Columbia River is the source of this component.

The processed TIMS image provides more insight into the distribution of the component materials (Figure 13). Figure 9 shows the location of the 6 TIMS band pass filters with respect to the spectral endmembers. As there is a significant spectral contrast between each of the spectral endmembers present, the TIMS data may be useful in distinguishing variations in the proportion of each of these endmembers.

TIMS bands 5, 3, and 1 are projected in the image as red, green, and blue respectively and it is possible to interpret composition based on the color of the image (Figures 9, 11). As the granodiorite endmember has a large absorption feature coincident with TIMS bands 1 and 3, the granodiorite is projected with relatively low blue and green and a relatively high red level resulting in a red color on the image. The basaltic endmember has a large silicate absorption feature at longer wavelengths coincident with bands 3 and 5 and is consequently a blue color on the TIMS image.

Interdune areas consist primarily of vegetation and ash deposits from the Mt. St. Helens eruption. Both of these materials are relatively featureless in the TIMS wavelength range compared to the dune spectral endmembers and, as a result of the decorrelation stretch, are projected as green on the image. The soil, which does not

contain the same spectral signature as the recovered clay endmember, contains an absorption that is coincident with band 1 and is yellow-orange on the TIMS image.

Immediately noticeable in the TIMS image is a considerable compositional variation within each dune. The slipface and farthest portion of the stoss are blue, indicating a relatively basaltic composition. The crest and stoss immediately behind the crest varies from red to purple, indicating a variable, but relatively granodioritic composition. Immediately behind each of the dunes is an orange colored strip that represents the soil uncovered by the forward migration of the dune since the ash was deposited from the Mt. St. Helens eruption in 1980.

As with the laboratory compositional percentages, the TIMS data do not show any sign of a regional pattern of compositional distribution within the dune field. There is no noticeable increase in a granodioritic composition towards the possible source of the Columbia River sands to the west nor are there any interdune local concentrations of any of the endmembers. The majority of compositional variation is located within each dune.

Discussion

The application of the factor analysis and endmember recovery techniques has identified three components in the dune sand: basalt, granodiorite, and a minor clay component. Each of these components may be identified through comparison to common terrestrial rock and mineral spectra. The eigenvector and eigenvalue analyses as well as the ability to closely model spectra of all 39 dune samples using linear combinations of these three endmembers indicates that these components are combining in a linear

manner. Minerals within each component are varying in unison and are probably of similar grain size. While this may be expected for the basaltic component that is composed primarily of groundmass where crystal size is much smaller than grain size, it also holds true for the granodioritic component where crystal size is typically much larger than the grain size of the sand. This means that while the sand grains are individual minerals such as feldspar and quartz, they are likely of similar grain size and distributed by the wind in the same manner. As a result, their apparent composition is not skewed from the original source bedrock.

The spectral similarity between the isolated sand components and fresh surfaces of the larger clast size deposits and bedrock outcrops within the Grand Coulee indicates that these components are compositionally similar and may be linked. The abrasive nature of the dune environment continually scours grain surfaces providing relatively fresh, unaltered surfaces that are not available on the larger clast deposits. Even bedrock exposures, such as samples from steep cliff walls, tend to have more weathering on their surfaces than the dune sands. Light amounts of alteration products (<20 areal %), in the form of clays such as montmorillonite or iron smectite, are present and identifiable in the dune samples, however these products and their effects may be isolated from the other components. It is not clear if these alteration products are present as individual grains or as rinds or coatings on either the basalt or granodiorite grains. Because eolian environments actively keep themselves relatively free of dust, weathering products and vegetation, they provide an ideal surface for thermal infrared remote determination of composition.

The TIMS image (Figure 13) demonstrates the ability to distinguish between these dune components using a multispectral thermal imager using standard image processing techniques. The image format of this data set provides information on the distributions of the compositions that would otherwise be difficult to determine using either field observations or samples collected and analyzed in the laboratory. Although it is impossible to obtain precise compositions using the 6 band TIMS pixels, felsic versus mafic versus soil compositions may be distinguished and correlated with the isolated endmember component.

The lack of any regional concentrations of the granodiorite and basalt components within the dune field indicates that both compositions were most likely deposited simultaneously during flood events. It is not clear what the cause of the variation in composition of each of the 39 samples is, though a likely cause is local variations in particle size within each dune. As seen in Figure 13, though the general trend of intradune compositional variation is clear, there are also clearly minor deviations from this trend. There is no indication of a separate source of granodiorite. While the Columbia River is a potential source for the granodiorite sand and there are numerous local dunes in the region, its physical separation of ~20 km as well as the relative isolation of Columbia River dune sands make it an unlikely source. In addition there is no indication of increasing concentrations of granodiorite in the Moses Lake dune sands towards the Columbia River to the west (Figure 13). The granodioritic bedrock upstream from both the Columbia River and the Grand Coulee where they meet at the Coulee Dam is a source for both deposits.

The spectral similarity does not nessecarily prove common progeny, especially with common compositions such as basalt and granodiorite. However, the commonality of the mineralogies and the lack of a clear compositional trend combined with the source possibilities of the Columbia River or the Grand Coulee, more clearly points to the Grand Coulee as the source. There are clearly granodioritic source materials within the coulee, granodiortic clast deposits mixed with basaltic deposits, and no clear regional trend of sand composition nor any clear evidence that sand is being transported from the Columbia River. There is also no reason the the granodiorite concentration should increase in the upstream direction, since all of the sand, basaltic and granodioritic, from the outflow floods will have been deposited simultaineously regardless of where it was picked up within the Grand Coulee.

Subsequent development of the dune field has separated the basalt and granodiorite components within each dune. The basalt has higher concentrations at grain sizes larger than 250μm and the granodiorite shows higher concentrations at grain sizes less than 250μm. This allows the wind, which preferentially concentrates smaller particle sizes at the crest of the dune, to separate the two initially well-mixed compositions within each dune. As a result, the basaltic component has higher concentrations on the slipface and rearward portion of the stoss while the granodiorite displays higher concentrations on and near the crest of the dune. The longer transport distance to the granodioritic source may account for its generally smaller particle size distribution.

This wind driven separation of compositions can be seen in TIMS images of several other dune fields. Though there are clearly distinguishable sources of materials in the

Kelso dune field in the Mojave Desert in California [*Ramsey et al.*, 1999], the images also display significant compositional variation within the individual dunes. This phenomenon is also clearly visible in datasets from the Great Sand Dunes in Colorado as well as Christmas Valley in Oregon [*Edgett* and *Christensen*, 1995]. This variation may help isolate and identify source lithologies and transport histories in regions where there is no regional pattern of compositional distribution or there is limited coverage of remote sensing data or sample collection.

In isolated regions or on other planets where it may be impossible to sample or even view potential bedrock sources, the similarity of the spectra of sand and source materials allows for the identification of the composition of the local or regional bedrock [e.g. *Bandfield et al.* 2000a; *Christensen et al.*, 2000a,b,c]. This is essential for determining the volcanic history of the Martian surface where basaltic and andesitic sands may be linked to bedrock that is often either covered or mantled.

Future higher spatial resolution instruments may be able to identify other compositions within each dune. THEMIS, which contains a 9 band, 100 m/pixel thermal infrared imager to fly on the 2001 Mars Odyssey orbiter will provide both the spatial and spectral resolution needed to determine if this compositional segregation occurs on Martian dunes. The mini-TES instrument, a 8 or 20 mrad field of view $10cm^{-1}$ spectral sampling spectrometer, will be carried on the 2003 Mars Exploration Rovers and have the potential to raster hyperspectral image cubes of the local scene. This sort of coverage will provide the ability to isolate and identify detailed compositions of multiple sand components, including source lithologies and any weathering products present. The TES

instrument has already shown variability in composition of intra-crater sands at the limit of its spatial resolution (~3 x 8 km) [*Wyatt* et al., 2001].

A wealth of Earth based thermal infrared datasets from both airborne and space platforms, such as TIMS, ASTER, and MASTER, are currently available for Earth remote sensing. These datasets along with the methodology presented here may be used to study and understand dune processes worldwide.

Conclusions

The application of thermal infrared remote sensing and laboratory spectroscopy as well as in situ field observations has demonstrated the following:

- Factor analysis and endmember recovery techniques can be applied to dune samples in order to isolate mineralogical sand components.
- The compositions of the isolated sand spectral components may be identified and linked to larger clast deposits as well as source bedrock lithologies.
- Weathering and coating components may also be isolated and identified in the dune sands although their concentrations are low (<20 areal %) due to abrasion in a vigorous eolian environment.
- While hyperspectral measurements are needed to obtain precise mineralogical compositions, multispectral thermal infrared imagers may clearly distinguish components and provide a rough estimate of composition.

- The Moses Lake sand dunes consist of significant amounts of both granodiorite and basalt compositions that were probably deposited simultaneously with no local concentrations of either composition. Both the basalt and granodiorite lithologies present in the Grand Coulee are compositionally similar to the larger clast sizes present on the Ephrata Fan as well as the components present in the sand.
- Subsequent development of the dune field has separated the basalt and granodiorite components within each dune. Dune crests contain higher concentrations of granodiorite than slipfaces and farthest portions of the stoss because smaller grain sizes (<250μm) contain higher concentrations of the granodiorite.
- While the Columbia River is a potential source for the granodioritic sand of the Moses Lake dunes, its physical separation (~20 km to the west) and the lack of increasing granodiorite concentrations towards the river make this possible source unlikely.
- These techniques are ideally suited for multi- and hyperspectral thermal infrared spectrometers and imagers such as ASTER, MASTER, TIMS, TES, THEMIS, and mini-TES for determining transport histories, weathering environments, and source lithologies.

References

Adams, J. B., M. O. Smith, P. E. Johnson, Spectral mixture modeling; a new analysis of rock and soil types at the Viking Lander 1 site, *J. Geophys. Res*., 91, 8098-8112, 1986.

Baker, V. R., and R. C. Bunker, Cataclysmic late Pleistocene flooding from glacial Lake Missoula: A review, *Quaternary Science Reviews, 4*, 1-41, 1985.

Bandfield, J.L., V.E. Hamilton, and P.R. Christensen, Martian Surface Compositions from MGS-TES, *Science*, in press 2000a.

Bandfield, J.L., P.R. Christensen, and M.D. Smith, Spectral dataset factor analysis and endmember recovery: Application to Martian atmospheric particulates, *J. Geophys. Res*., in press 2000b.

Berke, A., Bernstien, L.S., and Robertson, D.C., 1989 MODTRAN: A moderate-resolution for LOWTRAN 7: U.S. Air Force System Command, Geophysical Laboratory Report GL-TR-89-0122, 137 p.

Blount, G., M. O. Smith, J. B. Adams, R. Greeley, and P. R. Christensen, Regional aeolian dynamics and sand mixing in the Gran Desierto: Evidence from Landsat thematic mapper images, J. Geophys. Res., 95, 15,463-15,482, 1990.

Bretz, J H., The Lake Missoula floods and the Channeled Scabland, *Journal of Geology, 77*, 505-573, 1969.

Bretz, J H., H. T. U. Smith, and G. E. Neff, Channeled Scabland of Washington: New data and interpretations, *Geological Society of America Bulletin, 67*, 957-1049, 1956.

Christensen, P.R., J.L. Bandfield, M.D. Smith, and V.E. Hamilton, Identification of a basaltic component on the Martian surface from Thermal Emission Spectrometer data, *J. Geophys. Res.*, 2000a.

Christensen, P.R., J.L. Bandfield, V.E. Hamilton, D.A. Howard, M.D. Lane, J.L. Piatek, S.W. Ruff, W.L. Stefanov, A thermal emission spectral library of rock-forming minerals, *J. Geophys. Res.*, 2000b.

Christensen, P.R., J.L. Bandfield, R.N. Clark, K.S. Edgett, V.E. Hamilton, T. Hoefen, H.H. Kieffer, R.O. Kuzmin, M.D. Lane, M.C. Malin, R.V. Morris, J.C. Pearl, R. Pearson, T.L. Roush, S.W. Ruff, M.D. Smith, Detection of crystalline hematite mineralization on Mars by the Thermal Emission Spectrometer: Evidence for near-surface water, *J. Geophys. Res.*, 2000c.

Christensen, P.R., and S.T. Harrison, Thermal infrared emission spectroscopy of natural surfaces: Application to desert varnish coatings on rocks, *J. Geophys. Res.*, *98* (B11), 19,819-19,834, 1993.

Crowley, J.K., and S.J. Hook, Mapping playa evaporite minerals and associated sediments in Death Valley, California, with multispectral thermal infrared images, *J. Geophys. Res.*, *101*, 643-660, 1996.

Edgett, K.S., and P.R. Christensen, Multispectral thermal infrared observations of sediments in volcaniclastic aeolian dune fields: Implications for the Mars Global Surveyor Thermal Emission Spectrometer. *Proc. Lunar Planet. Sci. Conf.*, *26*, 1995.

Edgett, K. S., M. S. Ramsey, and P. R. Christensen, Aeolian erosion, transport, and deposition of volcaniclastic sands among the Shifting Sand Dunes, Christmas Lake

Valley, Oregon: TIMS image analysis, Summaries of the Fifth Annual JPL Airborne Earth Science Workshop, 2. TIMS Workshop, Jet Propulsion Laboratory Publication 95-1, v. 2, pp. 13-16, 1995.

Edgett, K.S., J.W. Rice, Jr., and V. R. Baker, Field trips accompanying the Mars Pathfinder Landing Site II Workshop: Channeled Scabland and Lake Missoula Break-out areas in Washington and Idaho, in *Mars Pathfinder Landing Site Workshop II: Characteristics of the Ares Vallis region and Field Trips in the Channeled Scabland, Washington*, edited by M. P. Golombek, K. S. Edgett, and J.W. Rice, Jr., LPI Technical Report, 95-01, pp. 31–63, Lunar and Planetary Institute, Houston, Texas, 1995.

Edgett, K. S., The Sand Component of the Modern Martian Aeolian Sedimentary System, Ph.D. Dissertation, Arizona State University, Tempe, 201 p., 1994a.

Edgett, K.S., The basaltic aeolian dunes near Moses Lake, Washington, U.S.A.: Changes in twentieth century activity moderated by local human and volcanic influences (abstract), in *Workshop on the Response of Eolian Processes to Global Change*, Occasional Papers, 2, pp. 33-35, Quaternary Sciences Center, Desert Research Institute, Reno, Nevada, 1994b.

Edgett, K.S. and N. Lancaster, Volcaniclastic aeolian dunes: Terrestrial examples and application to martian sands, *Journal of Arid Environments*, *25*, 271-297, 1993.

Edgett, K. S., and P. R. Christensen, The particle size of martian aeolian dunes, J. Geophys. Res., 96, 22,765-22,776, 1991.

Feely, K.C., and P.R. Christensen, Quantitative compositional analysis using thermal emission spectroscopy: Application to igneous and metamorphic rocks, *J. Geophys. Res.,104*, 24,195-24,210, 1999.

Gillespie, A.R., Spectral mixture analysis of multispectral thermal infrared images, *Remote Sens. Environ., 42*, 137-145, 1992.

Gillespie, A.R., Kahle, A.B., and Walker, R.E., Color enhancement of highly correlated images: I. Decorrelation and HSI contrast stretches, *Remote Sens. Environ., 20*, 209-235, 1986.

Golombek, M. P., R. A. Cook, H. J. Moore, and T. J. Parker, Selection of the Mars Pathfinder landing site, J. Geophys. Res., 102, 3967-3988, 1997.

Golombek, M. P., H. J. Moore, A. F. C. Haldeman, T. J. Parker, and J. T. Schofield, Assessment of Mars Pathfinder landing site predictions, J. Geophys. Res., 104, 8585-8594, 1999.

Grolier, M. J., and J. W. Bingham, Geologic map and sections of parts of Grant, Adams, and Franklin Counties, Washington, 1:62,500 scale, *U. S. Geological Survey Miscellaneous Investigations Series Map I-589*, 1971.

Gulick, C. W., Geologic map of the Moses Lake 1:100,000 Quadrangle, Washington, *Washington Division of Geology and Earth Resources Open File Report, 90-1*, 1990.

Holbrook, S. H., *The Columbia*, 393 p., Rinehart and Co., New York, 1956.

Hook, S.J., K.E. Karlstrom, C.F. Miller, and K.J.W. Mc Caffrey, Mapping the Piute Mountains, California, with thermal infrared multispectral scanner (TIMS) images, *J. Geophys. Res., 99*, 15,605-15,622, 1994.

Kahle, A.B., Surface emittance, temperature, and thermal inertia derived from Thermal Infrared Multispectral Scanner (TIMS) data for Death Valley, California, *Geophysics*, *52*, 858-874, 1987.

McKee, E. D., Introduction to a study of global sand seas, in A Study of Global Sand Seas, edited by E. D. McKee, pp. 1-19, U. S. Geol. Surv. Prof. Paper 1052, 1979.

Malinowski, E.R., *Factor Analysis in Chemistry*, 2nd ed., John Wiley & Sons, New York, 1991.

Nummedal, D., Field trip stop descriptions, In *The Channeled Scabland: A Guide to the Geomorphology of the Columbia Basin, Washington, A Comparative Planetary Geology Field Conference in the Columbia Basin, June 5-8, 1978*, edited by V.R. Baker and D. Nummedal, pp. 131-168, NASA, Washington, DC, 1978.

Petrone, A., *The Moses Lake sand dunes*, M.S. Thesis, 89 pp., Washington State University, Pullman, 1970.

Ramsey, M.S., and J.H. Fink, Estimating silicic lava vesicularity with thermal remote sensing: a new technique for volcanic mapping and monitoring, *Bull. Volcanol.*, *61*, 32-39, 1999.

Ramsey, M.S., P.R. Christensen, N. Lancaster, and D.A. Howard, Identification of sand sources and transport pathways at Kelso Dunes, California using thermal infrared remote sensing, *Geol. Soc. Am. Bull.*, *111*, 636-662, 1999.

Ramsey, M.S., and P.R. Christensen, Mineral abundance determination: Quantitative deconvolution of thermal emission spectra, *J. Geophys. Res.*, *103*, 577-596, 1998.

Rice, J.W., Jr., and K.S. Edgett, Catastrophic flood sediments in Chryse Basin, Mars, and Quincy Basin, Washington: Application of sandar facies model, *Journal of Geophysical Research, 102*, 4185-4200, 1997.

Rice, J.W., Jr., and K.S. Edgett, A sojourner's prospectus: Provenance of flood-transported clasts at the Mars Pathfinder landing site (abstract), in *Mars Pathfinder Landing Site Workshop II: Characteristics of the Ares Vallis region and Field Trips in the Channeled Scabland, Washington*, edited by M. P. Golombek, K. S. Edgett, and J.W. Rice, Jr., LPI Technical Report, 95-01, pp. 25-26, Lunar and Planetary Institute, Houston, Texas, 1995.

Ruff, S., P.R. Christensen, P.W. Barbera, and D.L. Anderson, Quantitative thermal emission spectroscopy of minerals: A technique for measurement and calibration, *J. Geophys. Res., 102*, 14,899-14,913, 1997.

Sarna-Wojcicki, A. M., S. Shipley, R, B Waitt, Jr., D. Dzurisin, and S. H. Wood, Areal distribution, thickness, mass, volume, and grain size of air-fall ash from the six major eruptions of 1980, in *The 1980 Eruptions of Mount St. Helens*, edited by P.W. Lipman and D. R. Mullineaux, U.S. Geological Survey Professional Paper, 1250, 577-600, 1981.

Smith, G. D., Sedimentology, stratigraphy, and geoarchaeology of the Tsulim Site, on the Hanford Site, Washington, M.S. Thesis, 169 p., Washington State University, Pullman, 1992.

Stetler, L. D., *Eolian dynamics and Holocene sedimentation at the Hanford Site, Washington*, Ph.D. Dissertation, 181 p., Washington State University, Pullman, 1993.

Stoffel, K. L., N. L. Joseph, S. Z. Waggoner, C. W. Gulick, M. A. Korosec, and B. B. Bunning, *Geologic map of Washington; Northeast Quadrant*, Washington Department of Natural Resources, Olympia, 36p., 1991.

Thomson, J.L., and J.W. Salisbury, The mid-infrared reflectance of mineral mixtures (7-14μm), *Remote Sens. Environ., 43*, 1-13, 1993.

Waitt, R. B., J. E. O'Connor, and G. Benito, Scores of gigantic, successively smaller Lake Missoula floods through the Channeled Scabland and Columbia Valley, in *Geologic Field Trips in the Pacific Northwest: 1994 Geological Society of America Annual Meeting*, edited by D.A. Swanson and R.A. Haugerud, sect. 1K, pp. 1-88, Geological Society of America, Boulder, Colorado, 1994.

Walters, K. L., and M. J. Grolier, *Geology and ground water resources of the Columbia Basin Project Area, Washington, Volume 1*, State of Washington, Division of Water Resources, Water Supply Bulletin No. 8, 1960.

Weitz, C. M., and T. G. Farr, Effects of surficial modification processes on thermal infrared signatures in the arid Southwestern United States, *J. Geophys. Res., 97*, 4649-4665,1992.

Wyatt, M. B., J. L. Bandfield, H. Y. McSween Jr., and P.R. Christensen, Compositions of Low Albedo Intracrater Materials and Wind Streaks on Mars: Examination of MGS TES Data in Western Arabia Terra, *Proc. Lun. Planet. Sci. Conf. XXXII*, 32, CDROM, 2001.

Figures

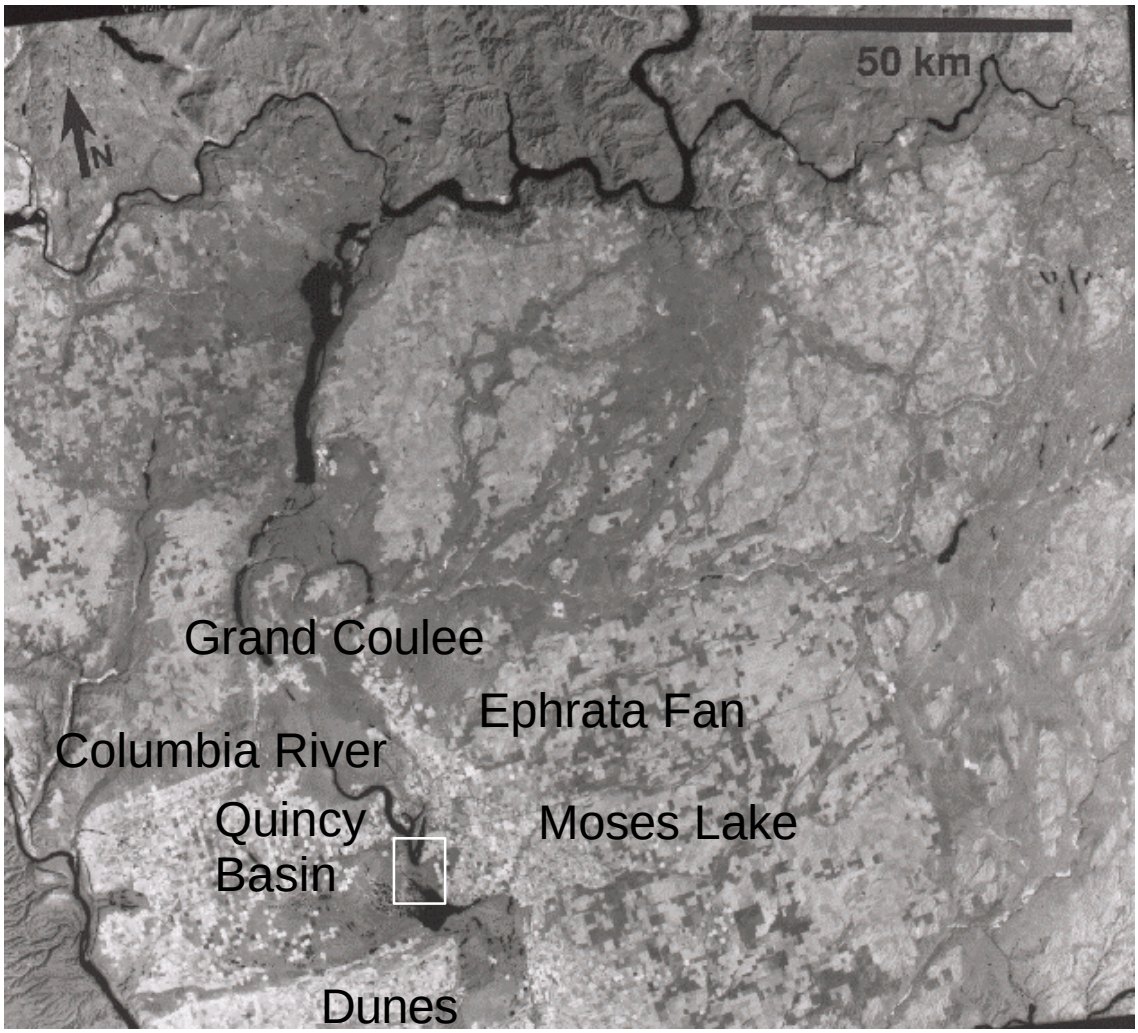

Figure 1. Regional view of the Quincy Basin and Grand Coulee in central Washington. The image is from the Landsat spacecraft taken on September 29, 1992. The white box indicates coverage of Figure 2 on the image. Center near 47º 27'N, 118º 49'W.

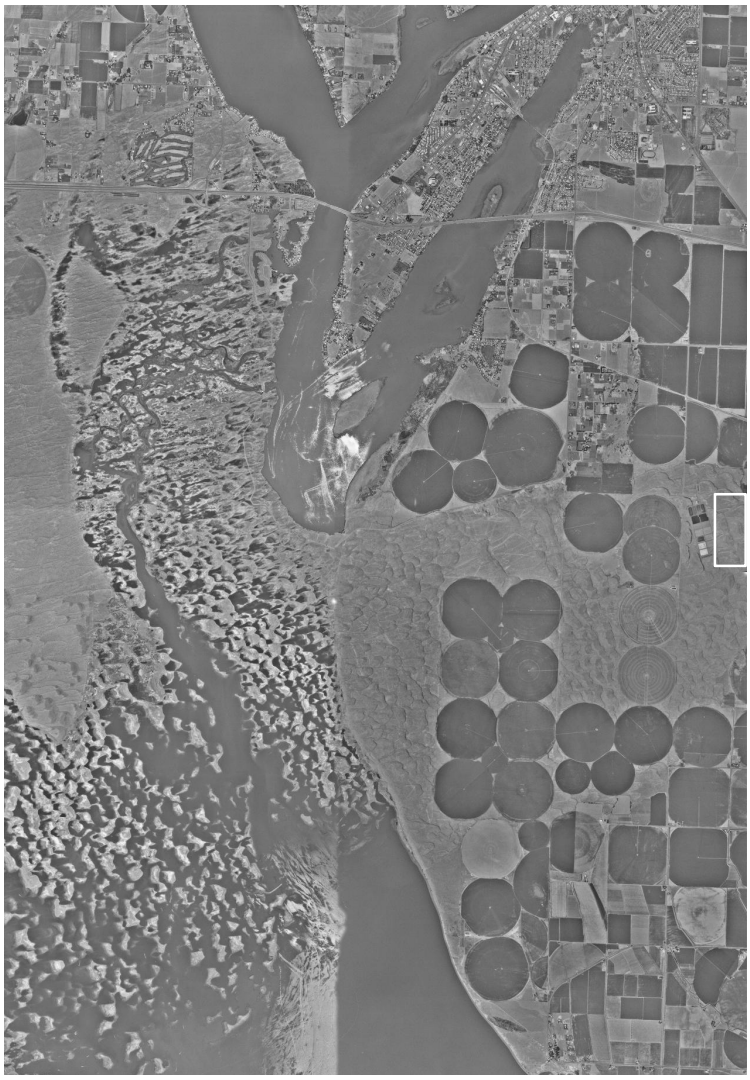

Figure 2. Aerial photograph of the Moses Lake Dunes. The Potholes Reservoir has flooded much of the dune field in the lower left portion of the image, creating islands out of individual dunes. The dune field itself naturally dams Moses Lake at the upper part portion of the image. The white box indicates coverage of Figure 13 on the image. Images are USGS digital orthophotos taken July 8 and 13, 1996, Moses Lake South, NW, NE, SW, and SE. Circular fields have a diameter of ~2/3 km.

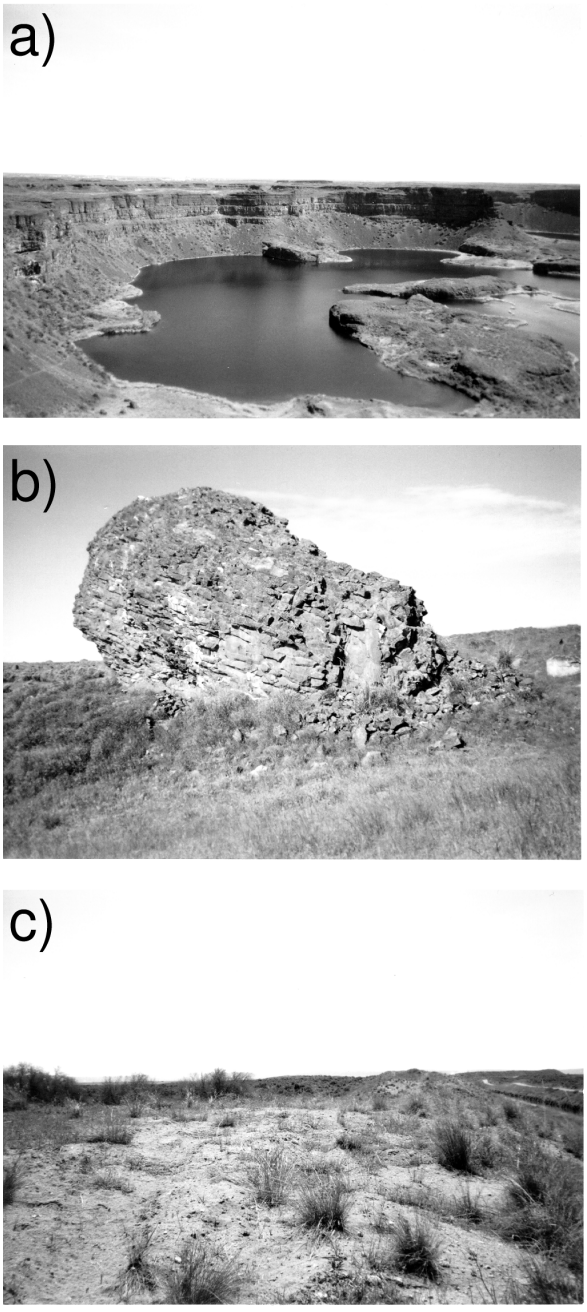

Figure 3. Field photographs of a) Grand Coulee (~0.5 km across), b) clasts on the Ephrata Fan (boulder is ~8 m high), and c) Moses Lake dune field (plants in foreground are ~0.5-1.0 m tall).

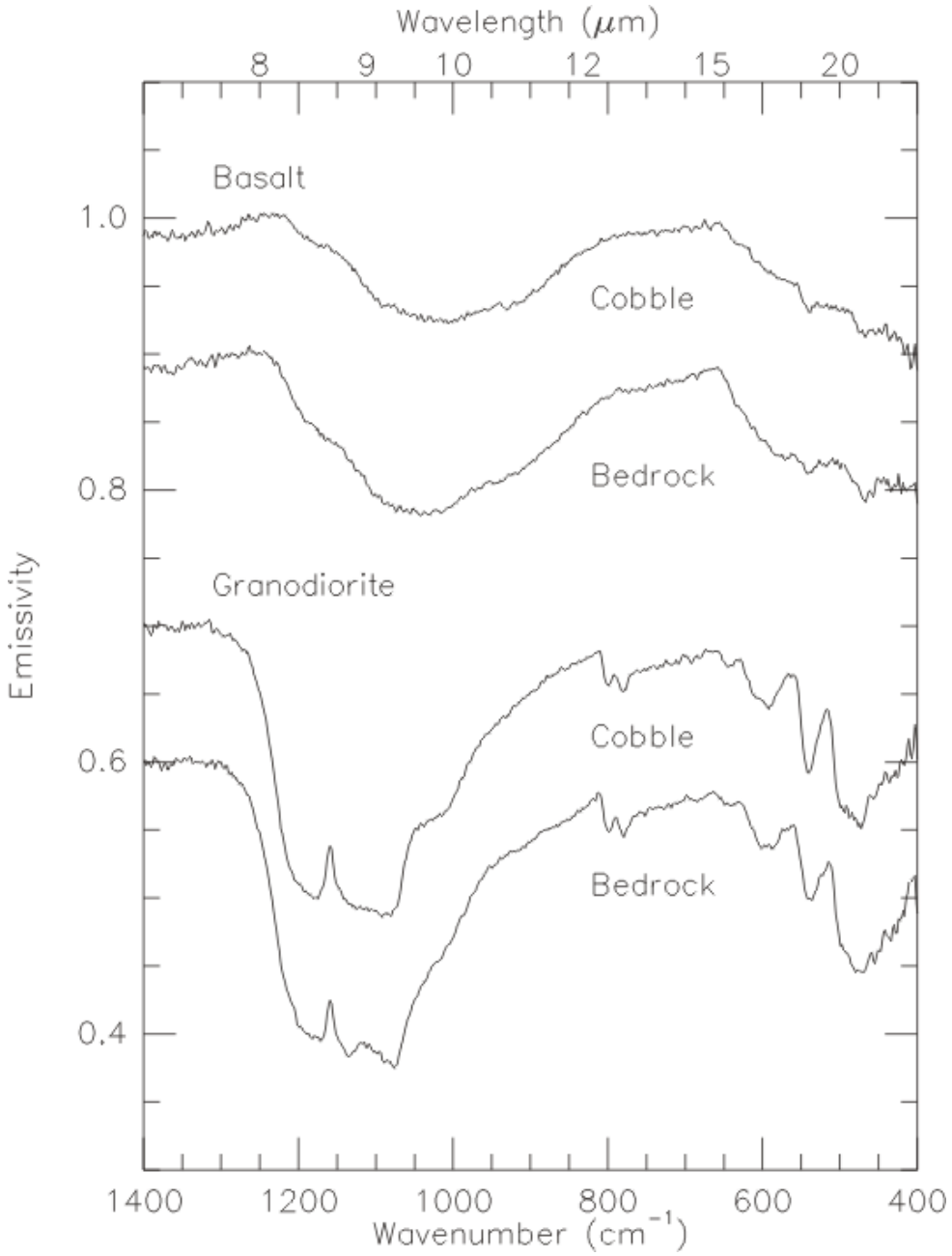

Figure 4. Basalt and granodiorite clast and bedrock sample spectra. Spectra were acquired from fresh surfaces of all samples. In both cases, the overall spectral signatures are similar indicating similar mineralogical compositions of both clasts and bedrock.

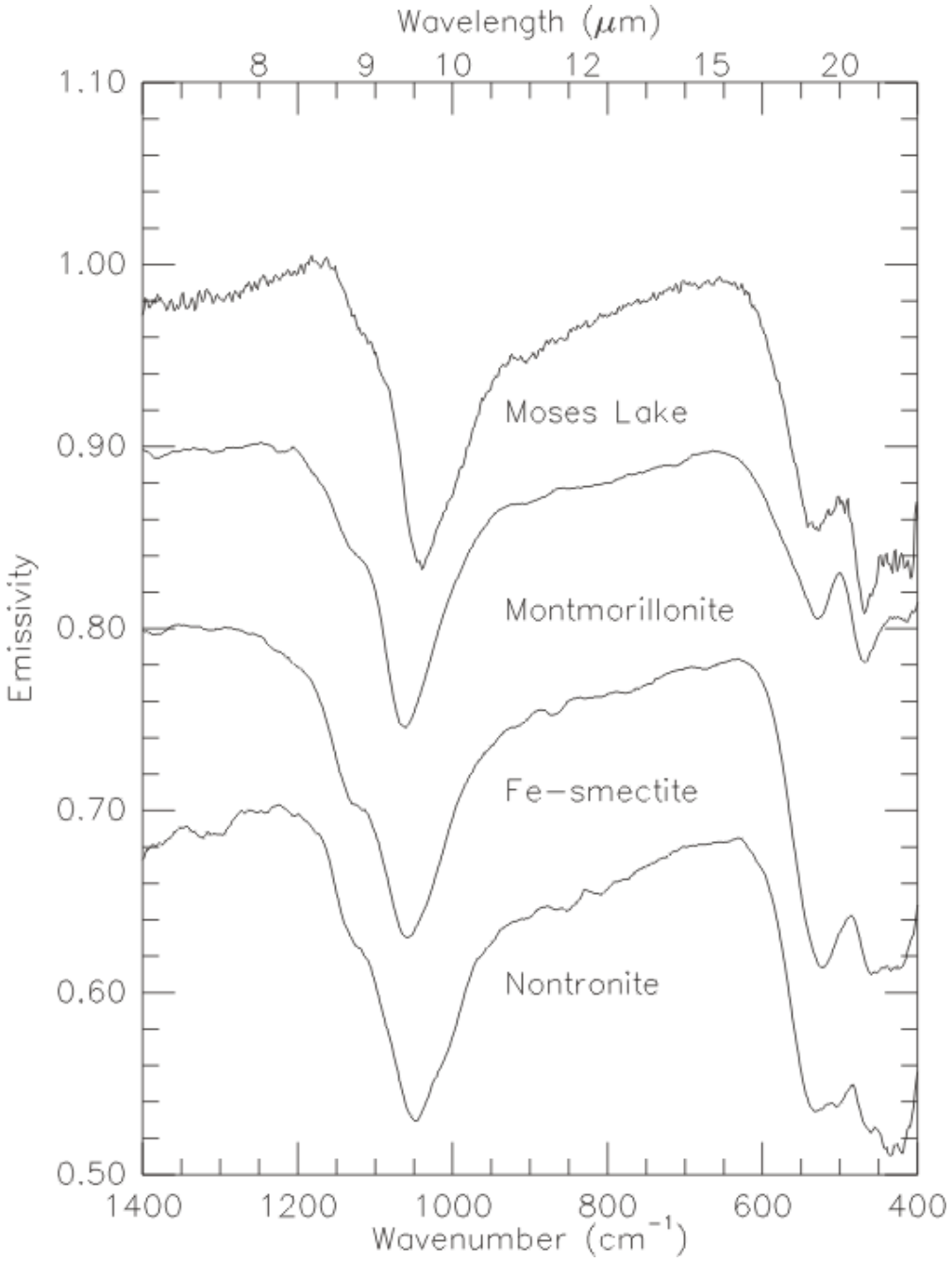

Figure 5. Spectrum of a buried clast surface within the Moses Lake area. This spectral signature compares very closely to several clay mineral spectra and represents a weathering product or coating in this region. Spectra are offset by 0.1 emissivity.

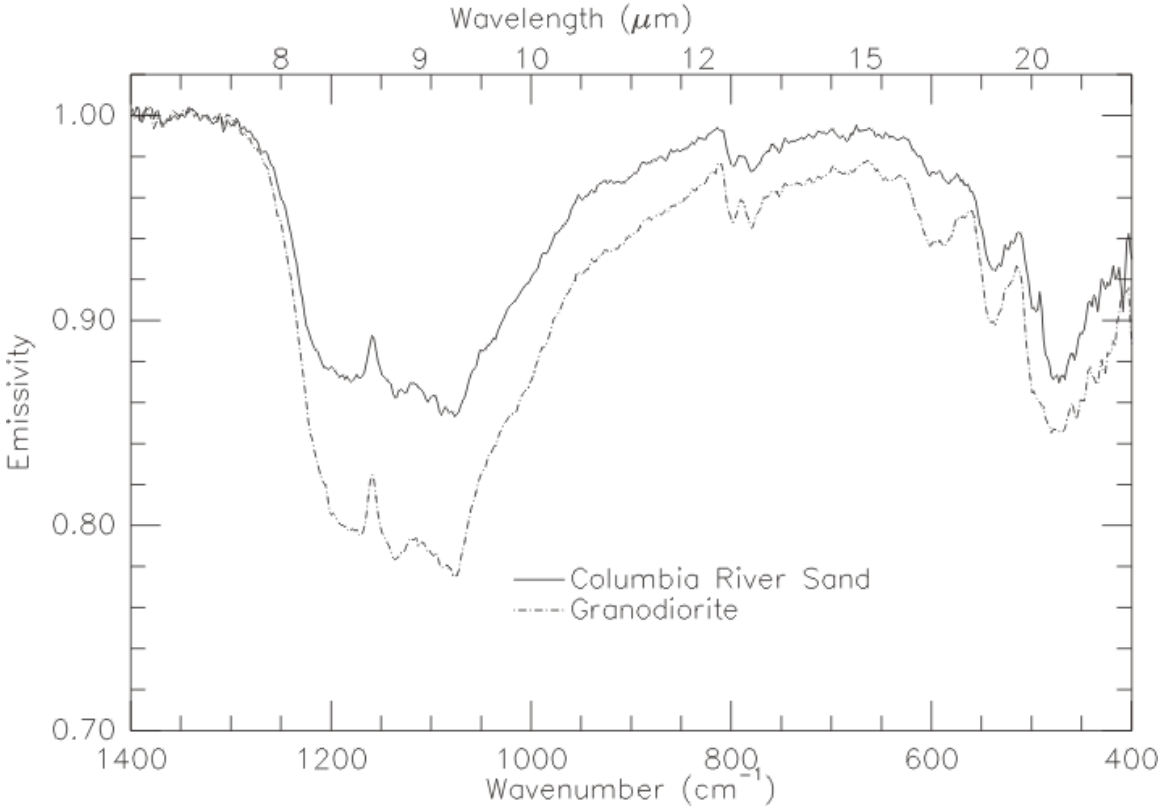

Figure 6. Spectrum of a Columbia River sand sample (solid) taken about 20 km west of the Moses Lake dune field. A sample of granodiorite (dashed) taken from an outcrop near Coulee Dam ~75 km north of Moses Lake is provided for comparison. All spectral features are matched well indicating that the mineralogical compositions are the same. The difference in contrast of the two spectra is due to physical differences between sand and broken rock surfaces.

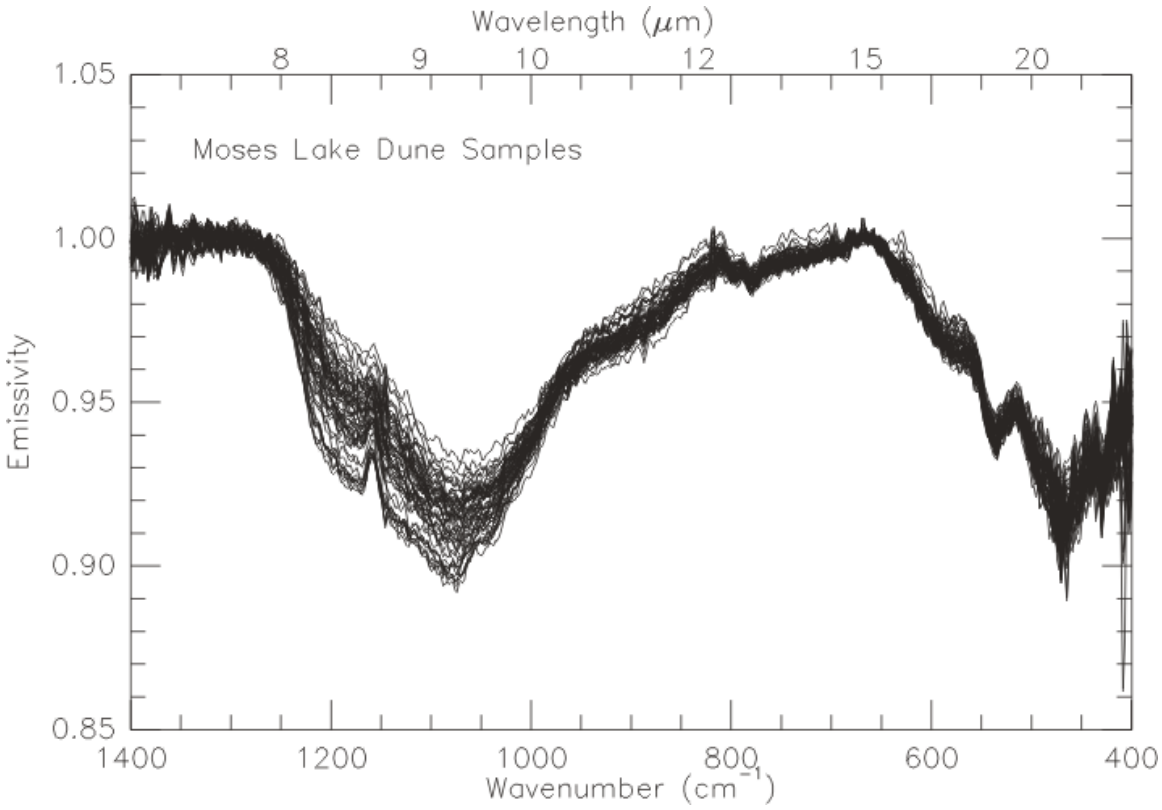

Figure 7. Set of 39 dune crest sample spectra used for the factor analysis and endmember recovery. Note the variation in the strength of the peak near 1150cm^{-1} due to variable amounts of quartz in the samples.

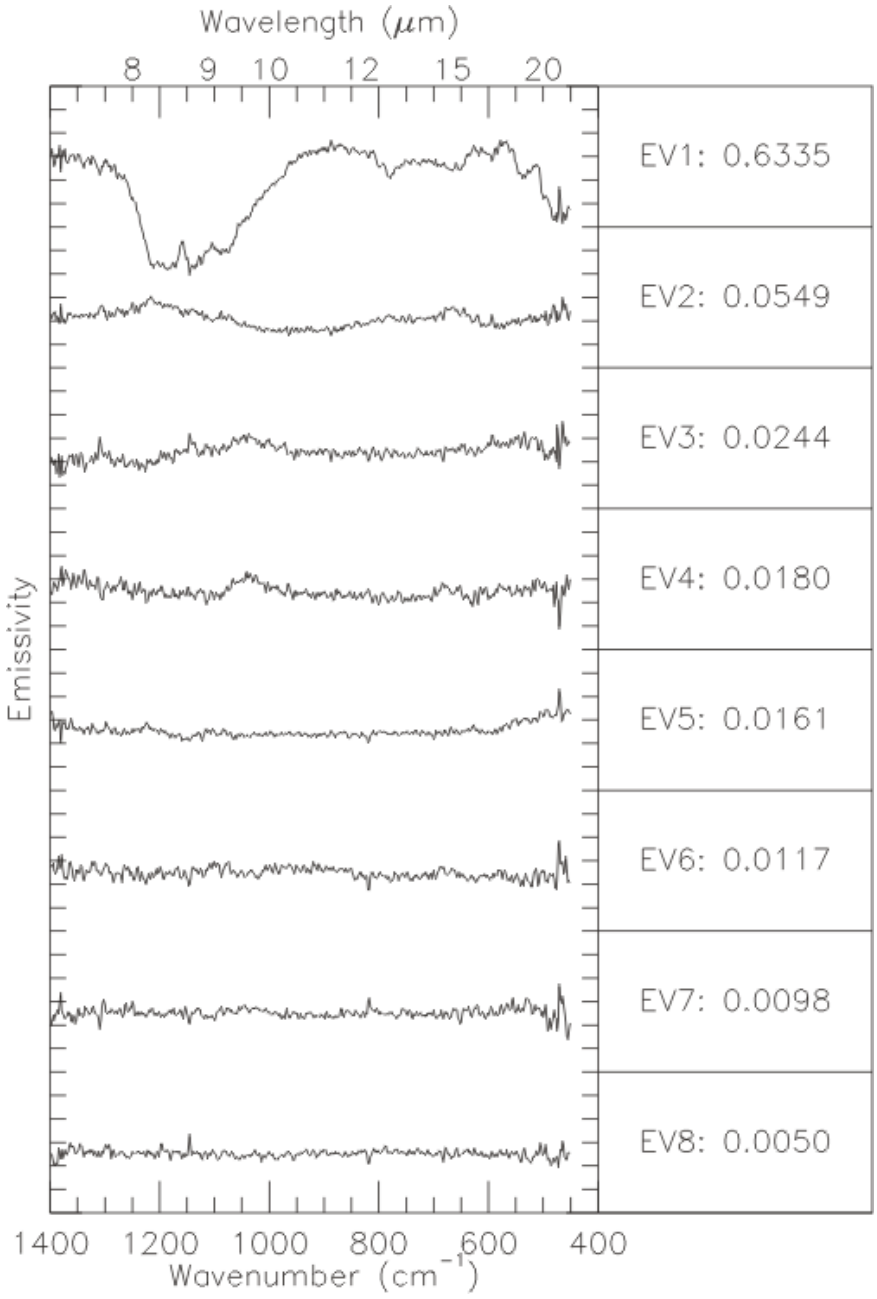

Figure 8. Eigenvectors and eigenvalues 1-8 (listed) derived for the 39 dune crest spectra. Minor spectral information is contained in eigenvectors 2-4. This minor information would be difficult to identify in the variance recorded by the eigenvalues.

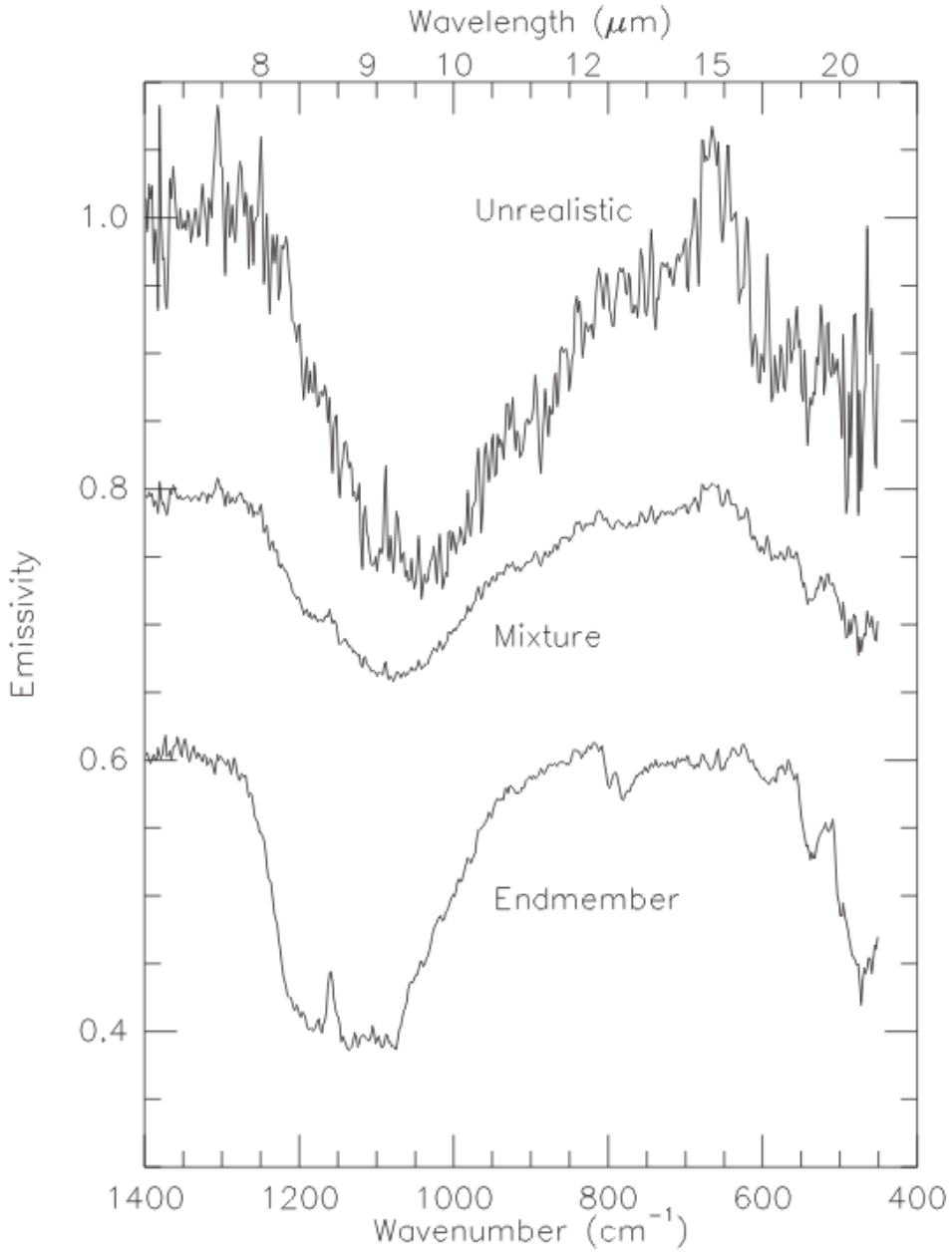

Figure 9. Example of predicted spectra returned from the endmember recovery technique. Unrealistic, mixture, and correct endmember predictions must be manually selected, but may be checked to ensure their accuracy. Spectra are offset by 0.2 emissivity.

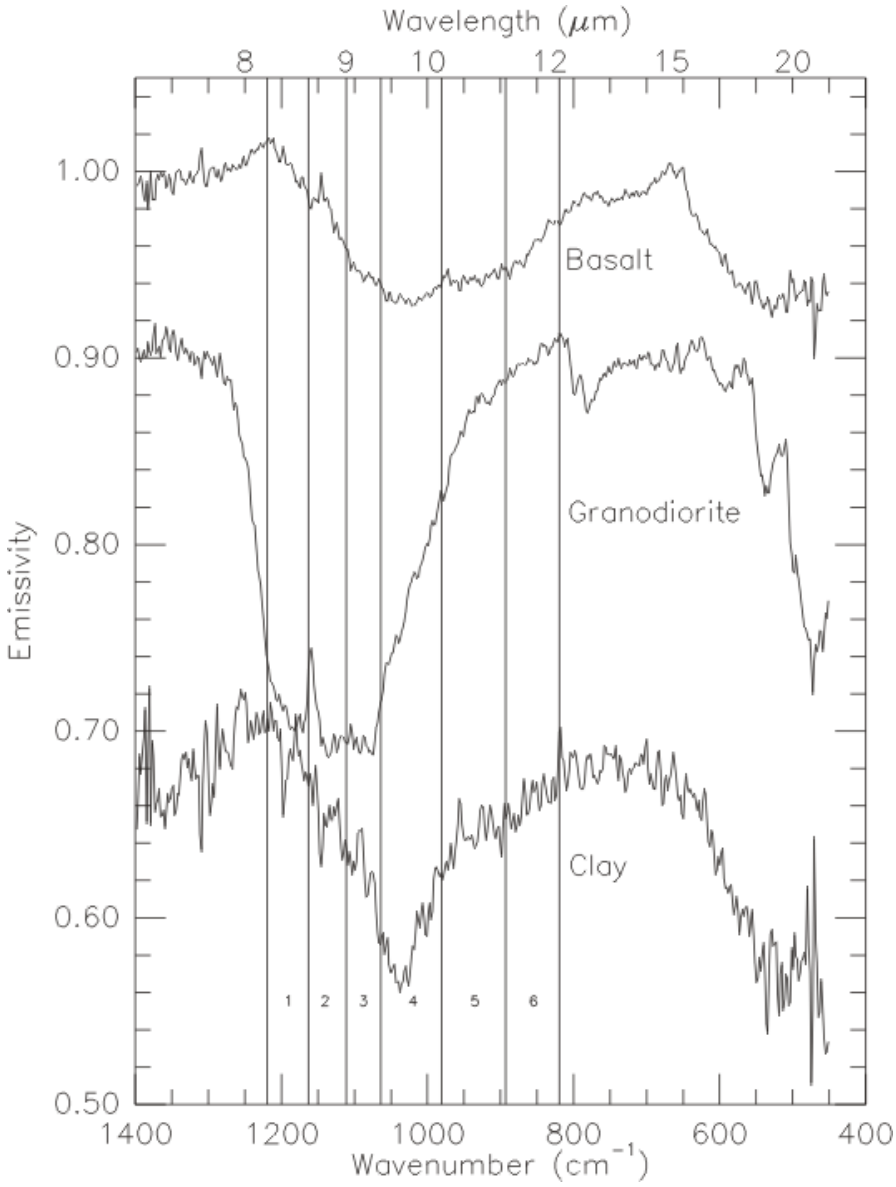

Figure 10. Endmembers recovered from the dune crest spectral set. Basalt and granodiorite are cleanly separated. The clay endmember is recovered, but is noisy as it is only present at <19% concentrations and only has 15% variability in the spectra. The granodiorite is offset by 0.1 and the clay is offset by 0.3 emissivity. The TIMS band passes are overlaid on the spectra for comparison to the image shown in Figure 11.

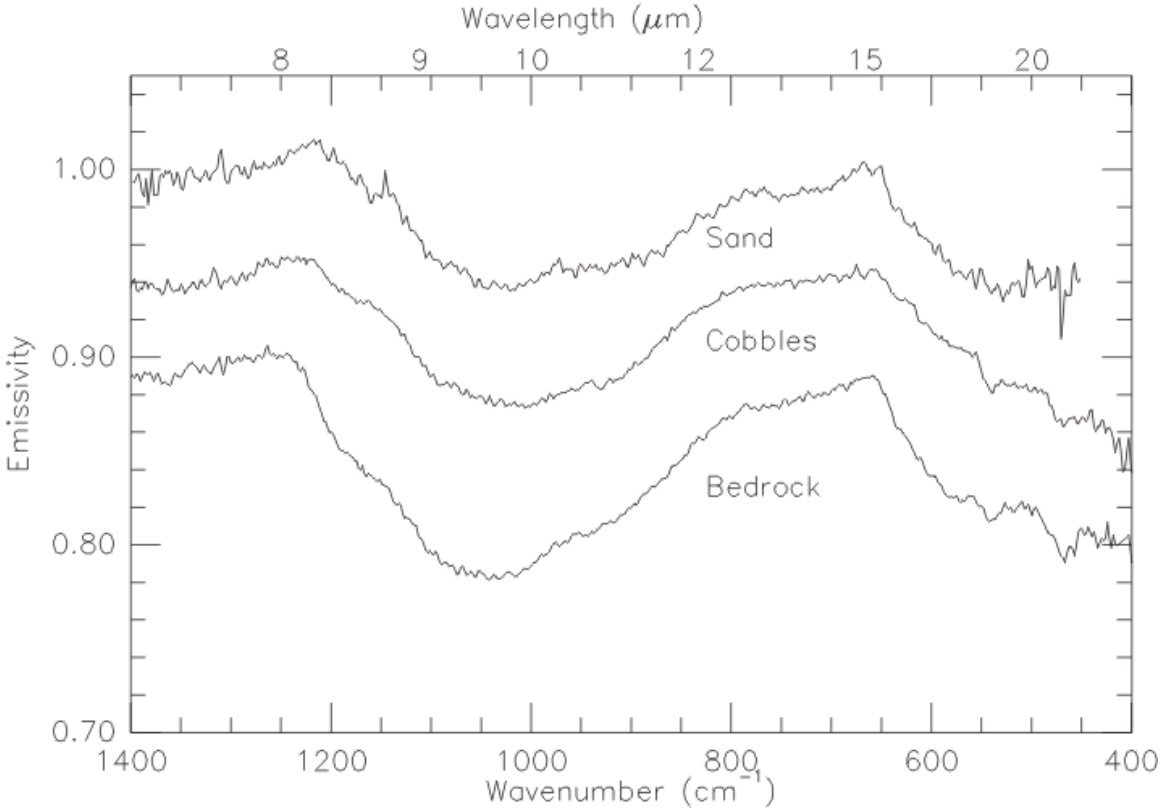

Figure 11. Recovered endmembers compared directly with samples in the Ephrata and Grand Coulee areas. All three recovered spectra match local materials and source lithologies.

(a) Recovered (sand), clast (cobbles), and bedrock spectra of the basaltic composition.

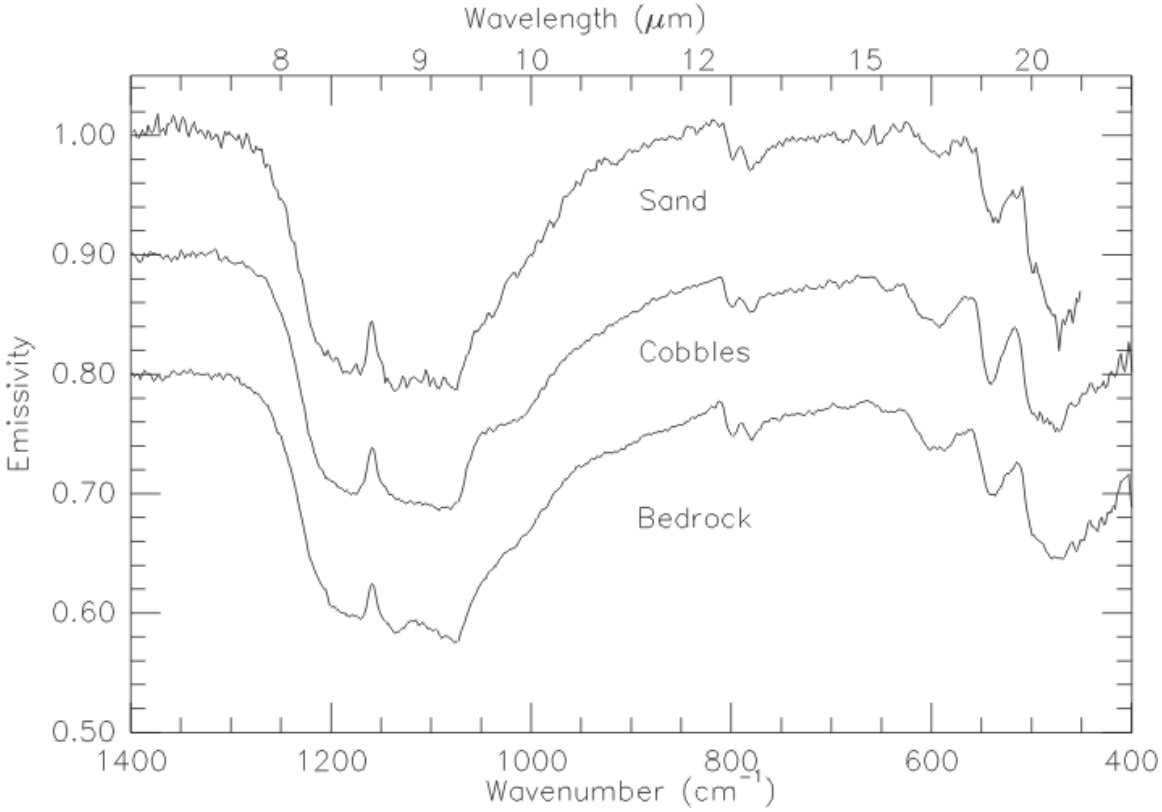

Figure 11, cont.

(b) Recovered (sand), clast (cobbles), and bedrock spectra of the granodioritic composition.

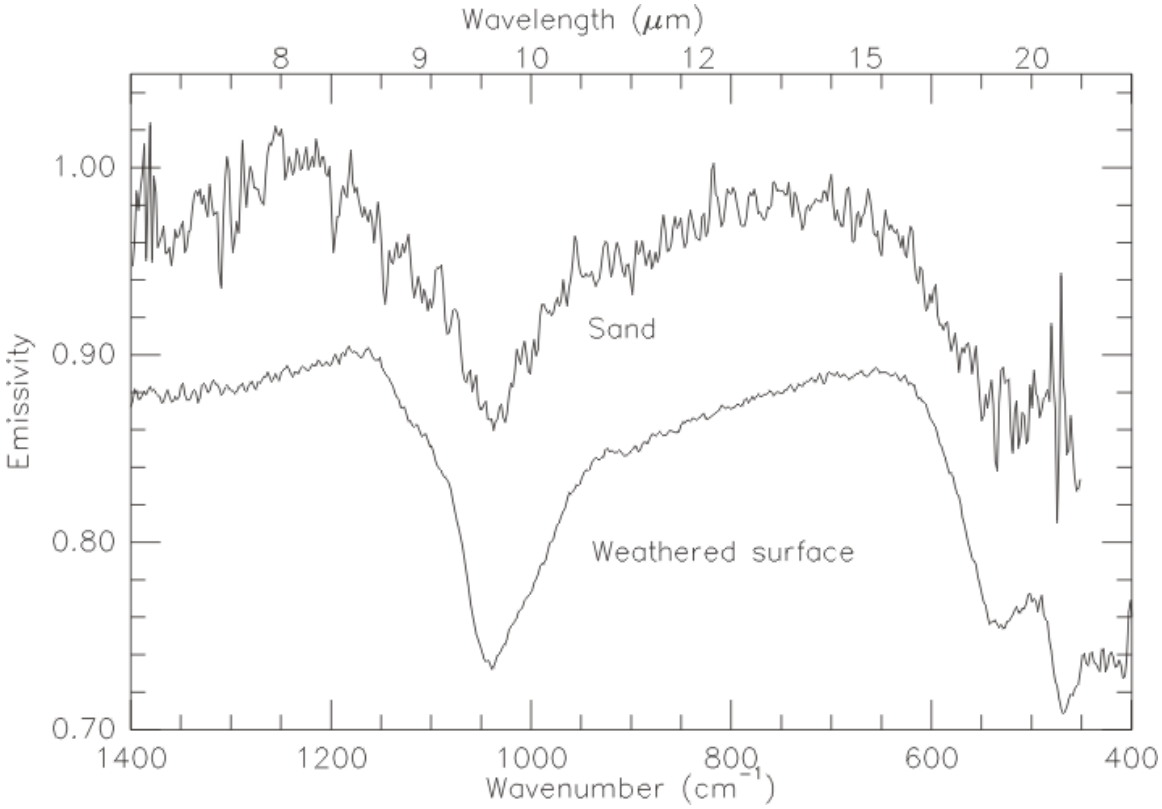

Figure 11, cont.

(c) Recovered (sand) and weathered surface of the buried cobble (shown in Figure 4).

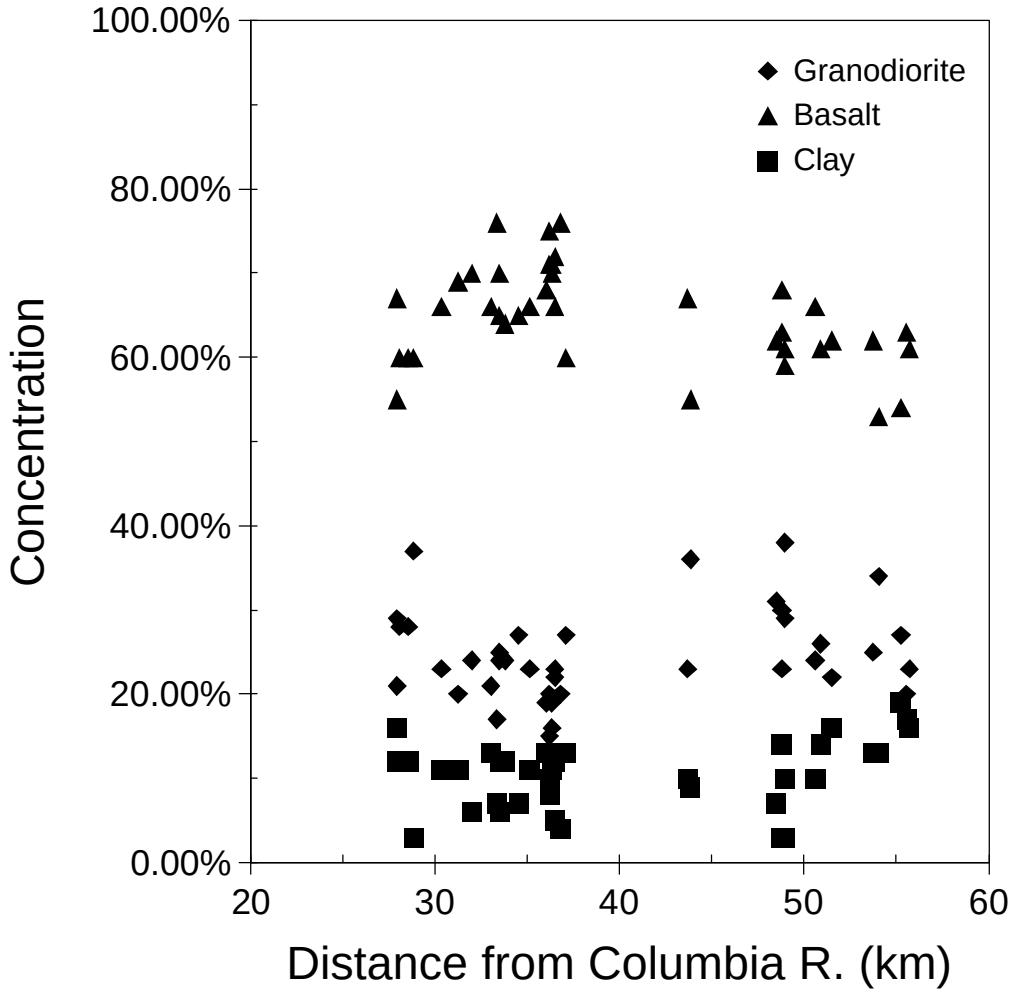

Figure 12. Component concentrations of individual dune samples plotted against the distance from the Columbia River.

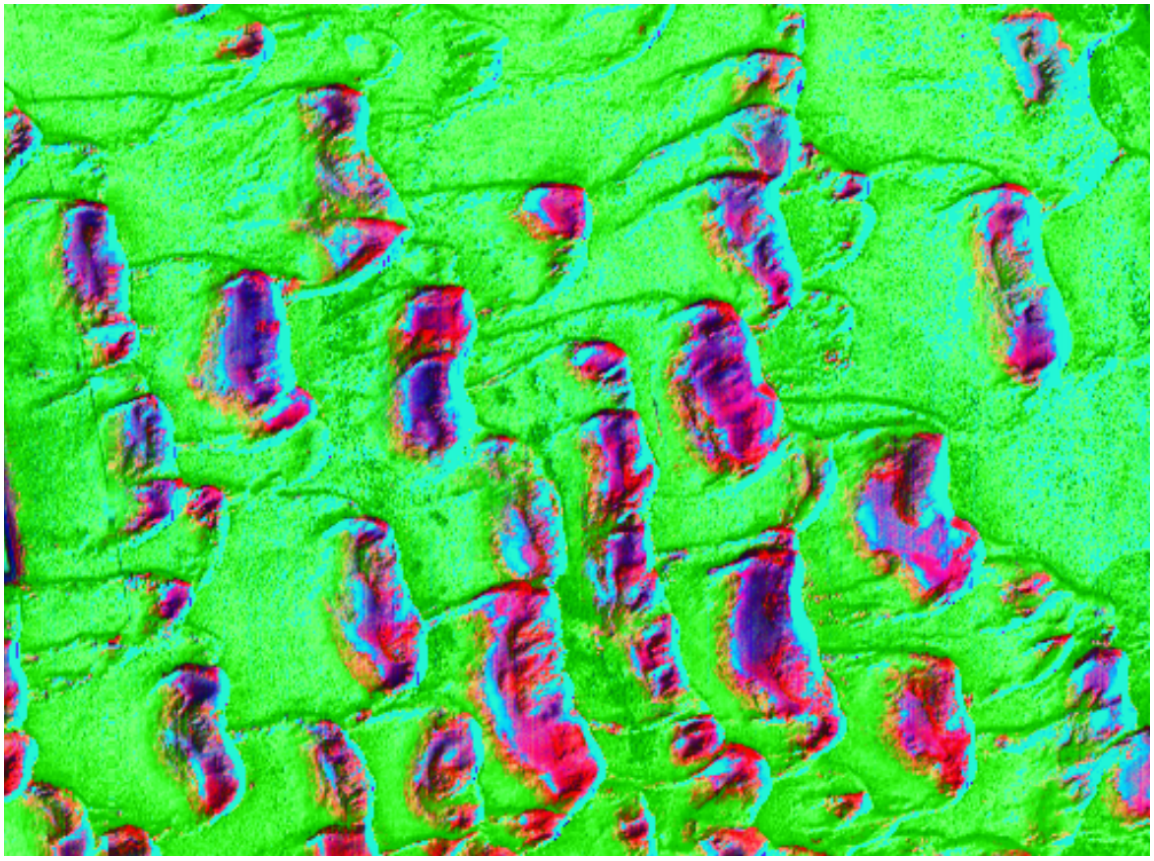

Figure 13. TIMS decorrelation stretch (bands 5-3-1 projected as red, green, and blue) image of a portion of the Moses Lake dune field. Green areas represent volcanic ash from the Mt. St. Helens eruptions. Yellowish areas represent bare soil uncovered by the forward migration of the dune since the 1980 eruptions. Red colors represent relative concentrations of granodiorite and blue represents relative concentrations of basalt. The compositional variation within each dune greatly exceeds that between the dunes. The image is approximately 1 km across.

Table 1. Deconvolution results for the set of 39 dune crest samples.

Sample	GD Conc	Basalt Conc	Clay Conc.	Sum	RMS Error
1	21%	67%	12%	100.15%	0.0018
2	28%	60%	12%	100.03%	0.0020
3	28%	60%	12%	99.98%	0.0020
4	29%	55%	16%	100.03%	0.0020
5	23%	72%	5%	99.99%	0.0021
6	22%	66%	12%	100.00%	0.0019
7	16%	71%	13%	100.04%	0.0014
8	20%	71%	8%	99.79%	0.0024
9	15%	75%	10%	100.12%	0.0020
10	23%	66%	11%	99.93%	0.0018
11	19%	70%	11%	99.88%	0.0016
12	20%	76%	4%	100.04%	0.0020
13	20%	69%	11%	100.04%	0.0018
14	23%	66%	11%	100.16%	0.0015
15	24%	70%	6%	100.15%	0.0019
16	21%	66%	13%	100.19%	0.0017
17	24%	65%	12%	100.23%	0.0020
18	24%	64%	12%	99.98%	0.0020
19	27%	65%	7%	100.10%	0.0019
20	19%	68%	13%	100.20%	0.0018
21	27%	60%	13%	99.99%	0.0022
22	37%	60%	3%	100.18%	0.0013
23	17%	76%	7%	100.10%	0.0015
24	25%	70%	6%	100.10%	0.0015
25	23%	67%	10%	100.08%	0.0023
26	31%	62%	7%	100.07%	0.0014
27	29%	61%	10%	99.98%	0.0019
28	38%	59%	3%	100.09%	0.0013
29	30%	68%	3%	100.03%	0.0010
30	23%	63%	14%	100.07%	0.0017
31	26%	61%	14%	100.42%	0.0022
32	24%	66%	10%	100.01%	0.0019
33	22%	62%	16%	100.21%	0.0017
34	25%	62%	13%	100.18%	0.0020
35	34%	53%	13%	99.96%	0.0027
36	27%	54%	19%	100.30%	0.0013
37	20%	63%	17%	100.17%	0.0019
38	23%	61%	16%	99.98%	0.0027
39	36%	55%	9%	100.02%	0.0017

Table 2: Deconvolution results for size fractions of a single dune crest sample.

Size Fraction	GD Conc.	Basalt Conc.	Clay Conc.	Sum	RMS Error	Wt. %
<125μm	39.00%	52%	10%	100.52%	0.0033	6%
125-180	42%	53%	5%	100.35%	0.0039	17%
180-250	33%	54%	13%	100.45%	0.0037	14%
250-355	28%	63%	10%	100.27%	0.0026	36%
355-500	28%	63%	9%	100.59%	0.0024	20%
500-710	29%	60%	11%	100.28%	0.0035	6%